Available online at www.sciencedirect.com

ScienceDirect

Acta Materialia 74 (2014) 165–182

Acta MATERIALIA

www.elsevier.com/locate/actamat

Effect of ion irradiation on tensile ductility, strength and fictive temperature in metallic glass nanowires

D.J. Magagnosc [a], G. Kumar [b], J. Schroers [c], P. Felfer [d], J.M. Cairney [d], D.S. Gianola [a,*]

[a] Department of Materials Science and Engineering, University of Pennsylvania, Philadelphia, PA 19104, USA
[b] Department of Mechanical Engineering, Texas Tech University, Lubbock, TX 79409, USA
[c] Department of Mechanical Engineering and Materials Science, Yale University, New Haven, CT 06511, USA
[d] Australian Centre for Microscopy and Microanalysis, University of Sydney, NSW 2006, Australia

Received 13 February 2014; received in revised form 1 April 2014; accepted 1 April 2014

Abstract

Ion irradiation of thermoplastically molded $Pt_{57.5}Cu_{14.3}Ni_{5.7}P_{22.5}$ metallic glass nanowires is used to study the relationship between glass structure and tensile behavior across a wide range of structural states. Starting with the as-molded state of the glass, ion fluence and irradiated volume fraction are systematically varied to rejuvenate the glass, and the resulting plastic behavior of the metallic glass nanowires probed by *in situ* mechanical testing in a scanning electron microscope. Whereas the as-molded nanowires exhibit high strength, brittle-like fracture and negligible inelastic deformation, ion-irradiated nanowires show tensile ductility and quasi-homogeneous plastic deformation. Signatures of changes to the glass structure owing to ion irradiation as obtained from electron diffraction are subtle, despite relatively large yield strength reductions of hundreds of megapascals relative to the as-molded condition. To reconcile changes in mechanical behavior with glass properties, we adapt previous models equating the released strain energy during shear banding to a transit through the glass transition temperature by incorporating the excess enthalpy associated with distinct structural states. Our model suggests that ion irradiation increases the fictive temperature of our glass by tens of degrees – the equivalent of many orders of magnitude change in cooling rate. We further show our analytical description of yield strength to quantitatively describe literature results showing a correlation between severe plastic deformation and hardness in a single glass system. Our results highlight not only the capacity for room temperature ductile plastic flow in nanoscaled metallic glasses, but also processing strategies capable of glass rejuvenation outside of the realm of traditional thermal treatments.

Keywords: Metallic glass; Nanowire; Tensile ductility; Ion irradiation; Fictive temperature

1. Introduction

Since their discovery in 1960, metallic glasses (MGs) have garnered significant interest due to a suite of attractive properties [1]. In particular, the combination of metallic bonding and the absence of long-range order has produced materials with superior mechanical properties compared to their crystalline counterparts. MG alloys have demonstrated high elastic strain limits, high strengths, potential for high fracture toughness, good wear resistance and low mechanical dissipation [2,3]. Coupled with versatile processing through thermoplastic molding, the mechanical properties make MGs appealing for many structural applications, particularly at miniature length scales, such as those in microelectromechanical system (MEMS) devices [4–6].

Despite this promise, widespread applications of MG alloys as structural materials have been hampered by poor plastic performance and a tendency towards catastrophic failure at room temperature. Specifically, deformation in

* Corresponding author.
E-mail address: gianola@seas.upenn.edu (D.S. Gianola).

http://dx.doi.org/10.1016/j.actamat.2014.04.002
1359-6454/

metallic glasses at room temperature is characterized by a deleterious propensity for localized plastic shearing into thin bands, known as shear bands, that progress in a self-catalytic fashion and are incipient to final fracture [7]. Prior to such macroscopic level shearing, plastic deformation is understood to be accommodated by the activation of shear transformation zones (STZs) [8]. An STZ is a local collection of atoms that undergoes a cooperative shear rearrangement, the operation of which is biased under an applied shear stress [9]. While STZs have been shown to carry plasticity over all temperature ranges, the ensuing plastic response of MGs strongly depends on temperature and strain rate [10]. At temperatures close to the glass transition temperature (T_g), plastic deformation is homogeneous and can be adequately described by Newtonian flow [11]. At low temperatures relative to T_g and high strain rates, STZ operation leads to strain localization and the formation of shear bands [7].

However, such propensity for shear localization and its ubiquity in plastic deformation at room temperature have not been definitively linked to specific structural or compositional features. Many theories rely on order parameters, such as free volume [8,11] or effective temperature [12], to predict deformation modes. For instance, Argon's seminal work on STZs related deformation to the generation and annihilation of free volume during STZ operation [8]. During low-temperature deformation, the MG structure is unable to relax sufficiently rapidly and the free volume persists (or its rate of generation increases). As deformation proceeds, the strain rate localizes in the softer, dilated regions. However, free volume and effective temperature are often experimentally intractable or strongly sensitive to the measurement approach [13–17], thereby limiting their predictive capability for macroscopic experiments. Instead, a large portion of glass development has focused on improving intrinsic glass performance based on empirical evidence guided by semi-physical analytical modeling [18–21]. One example of a common strategy is the synthesis of MGs with high Poisson's ratio (or low μ/B), which has been linked to a large capacity for plastic deformation via facile shear band nucleation and propagation coupled with large resistance to cavitation and fracture [22,23].

However, within a given alloy, the properties and deformation mode depend strongly on processing conditions [24–26]. The loading modality also influences the mechanical response. Both yield stress and capacity for plasticity increase in confined loading geometries (i.e. compression or bending) as compared to uniaxial tension [27–29]. The increased plasticity is a result of the arrest of shear bands due to confinement. Various heat treatments influence the plastic response as well. Sub-T_g annealing has been shown to relax the glass structure. Structural relaxation leads to embrittlement in normally ductile glasses due to a reduction in shear band activity [25,30]. Subsequent annealing above T_g rejuvenates the structure and the glass regains its capacity for plastic deformation.

Recently this transition in mechanical behavior was rationalized by considering the fictive temperature (T_f) of the glass following distinct thermal treatments [31]. Fictive temperature is defined as the temperature at which the frozen-in liquid structure is at equilibrium [32]. By performing bending tests on MG samples prepared at different T_fs, an alloy-dependent critical fictive temperature (T_{fc}) was observed. A specimen prepared above T_{fc} exhibited plastic deformation in bending while a specimen prepared below T_{fc} responded in a brittle manner [31].

Similar to the thermal treatments mentioned before, mechanical deformation was shown to induce structural relaxation or rejuvenation of MGs. For instance, cyclic loading within the elastic regime was observed by Packard et al. [33,34] to lead to hardening of metallic glasses. Molecular dynamics simulations have provided insight into the observed hardening, with the hardening being attributed to relaxation of the glass structure and annihilation of free volume [35–37]. Interestingly, this indicated that plastic deformation occurred at the atomic scale, while the macroscopic behavior remains seemingly elastic. Conversely, severe plastic deformation was shown to rejuvenate MGs, leading to softening [28,38–42] as a result of large cumulative plastic shearing. The large strains required for such reported changes were achieved in MGs through confined loading techniques that accumulate large shear deformations, such as high-pressure torsion (HPT) [43]. Rejuvenation of MGs manifested as increased free volume, increased stored enthalpy, and reduced elastic modulus and hardness [39,41,42]. Furthermore, examining the indents of these severely deformed MGs showed a suppression of shear bands relative to the undeformed glass [42]. Similar changes have been reported following shot peening of MGs, producing a severely deformed surface layer on the order of 100 μm thick [44–46]. When measured parallel to the surface, the hardness was observed to decrease closer to the shot-peened surface, where the damage was expected to be most pronounced [44]. The softening due to shot peening was also associated with structural rejuvenation, as measured by increased stored enthalpy during calorimetric studies [46]. Thus, provided a given MG alloy, mechanical properties may be altered by various treatments (both thermal and mechanical); in some cases, a transition in plastic deformation mode was possible.

The structural changes created by thermal processing and severe mechanical treatments were remarkably similar to the bombardment of MGs with energetic particles [47]. Recent molecular dynamics studies of simulated ion irradiation in metallic glass have demonstrated a persistent, yet subtly different, amorphous structure as well as significant changes in mechanical response [48–50]. Mayr observed an increase in free volume and reduction of yield stress in irradiated MGs as compared to a more relaxed sample [48]. Xiao et al. observed a reduction in the fraction of icosahedral clusters coupled with a softening and delocalization of deformation in MG samples prepared by simulated casting [49]. A similar study by Avchaciov et al. also reported

changes in chemical and topological short-range order, as observed in the packing polyhedra; however, shear band suppression was not observed [50]. Experimental studies corroborate these atomistic simulations [51–54]. Softening due to ion irradiation was explicitly studied by Raghavan et al. in heavily irradiated micropillars [51]. In this study, a 30% reduction in yield stress was observed in heavily irradiated MG pillars. Liu et al. probed the influence of the focused ion beam (FIB), commonly used for the preparation of small-scale testing specimens, on the inhomogeneous to homogeneous transition by irradiating and indenting MG thin films [53]. This study demonstrated a suppression of shear banding and a reduction in the hardness of MG thin films subjected to FIB milling [53]. This indentation result was supported by Raghavan et al. in a Zr-based bulk MG subject to high-energy Ni^+ irradiation [52]. Furthermore, we recently reported a reversible transition between brittle-like and ductile-like states in Pt-based MG nanowires produced by a thermoplastic molding technique (without the FIB) [4,54]. By irradiating a pristine nanowire, tensile ductility was induced. Subsequent annealing under conditions known to fully relax the Pt-glass returned the nanowires to their initial brittle-like state. Our observation of increased tensile ductility due to FIB irradiation was recently supported by Chen et al. in a study of electroplated MGs [55]. A comparison of electroplated (FIB-free) tensile bars to FIB-fabricated specimens revealed an increase in plastic strain when the FIB was employed. Taken as a whole, ion irradiation appears to act as an agent for glass rejuvenation, resulting in enhanced plastic deformation and reduced strength and hardness reminiscent of the effects of employing an ultrahigh cooling rate from the molten alloy.

In contrast to the documented sensitivity of MGs to their processing history, such irradiation effects have been largely overlooked in recent micro- and nanoscale mechanical testing of MGs. The majority of micro- and nanomechanical testing has been performed on FIB-prepared specimens [56–65]. As the sample size decreased, a transition from heterogeneous to quasi-homogeneous deformation was observed [57,60,62]. While the behavior was rationalized based on energetic arguments for the size dependence of shear banding in analogy to Griffith crack propagation [60], the possible influence of the FIB on glass structure has not been considered. Yet, as was previously discussed, there is emerging evidence that irradiation strongly influences the mechanical response of MGs through structural changes, manifested as a decrease in yield stress. Furthermore, a recent report by Tian et al. showed that even electron irradiation used for imaging during *in situ* tensile experiments of MGs at high current densities enhanced the measured tensile ductility [65]. However, while attempts have been made to account for the effect of structural state in microscale MGs [61], no study to date has systematically investigated structure–property relationships under different ion irradiation conditions. Small volumes of MGs present a unique opportunity for such a study as the penetration depth of ions is relatively limited, precluding precise studies in bulk materials with small volume fractions of irradiated material. Moreover, the outcome of such a systematic study could provide insight to guide new processing strategies for tailoring of MG properties.

In this paper, we report on changes to the mechanical response of molded MG nanowires subjected to Ga^+ ion irradiation using FIB. By systematically varying the irradiated volume fraction and ion fluence, a transition from originally brittle-like to ductile-like tensile behavior was measured, a direct result of changes to the structural state of the glass. Above a threshold of ion fluence and irradiated volume fraction, the plastic response was characterized as more ductile, deformation became quasi-homogeneous and a reduction in yield stress was measured. The observed increase in ductility and reduction in yield stress are understood by changes in the fictive temperature of the MG caused by ion irradiation. Finally, we present a unified model for the scaling of yield strengths in MGs that is capable of describing the variety of structural states available to a given MG.

2. Experimental materials and methods

Nanomechanical testing was performed *in situ* on $Pt_{57.5}Cu_{14.3}Ni_{5.7}P_{22.5}$ nanowires. The Pt-glass nanowires were fabricated through thermoplastic molding, previously described in Ref. [4]. Briefly, the nanowires were molded in a nanoporous alumina template at 270 °C under an applied pressure of 130 MPa. After molding, the alumina template was etched in KOH to leave free-standing nanowires. The resulting nanowires had diameters between 90 and 160 nm, with nominal testing gage lengths of 3 μm.

The Pt-glass nanowires were subsequently mounted on specially prepared atomic force microscope (AFM) cantilevers. Using the FIB, the cantilever end was removed and trenches were milled parallel to the cantilever axis to aid in nanowire alignment. Using a nanomanipulator (Kleindiek) in a scanning electron microscope (SEM; FEI Quanta 600 FEG Mark II), nanowires were harvested and secured to the prepared cantilever using a Pt-based electron beam induced deposition (EBID) material.

Quantitative uniaxial tension nanomechanical tests were performed *in situ* in a dual beam SEM/FIB (FEI Strata DB235) using a custom testing platform, as described in Ref. [54]. The platform consisted of a closed-loop six degree of freedom nanopositioning (6 DOF) stage (SmarAct GmbH), a stiff linear piezoelectric actuator (Physik Instrumente) and a MEMS-based load cell (FemtoTools). The 6 DOF stage allowed for alignment of the sample and load sensor with nanometer accuracy. The actuator provided displacement control with a displacement range of 60 μm and sub-nanometer resolution. The load cell was capable of measuring forces up to 100 μN, with <10 nN noise under a high vacuum. Fig. 1 shows the nanowire harvesting process and the nanomechanical testing platform.

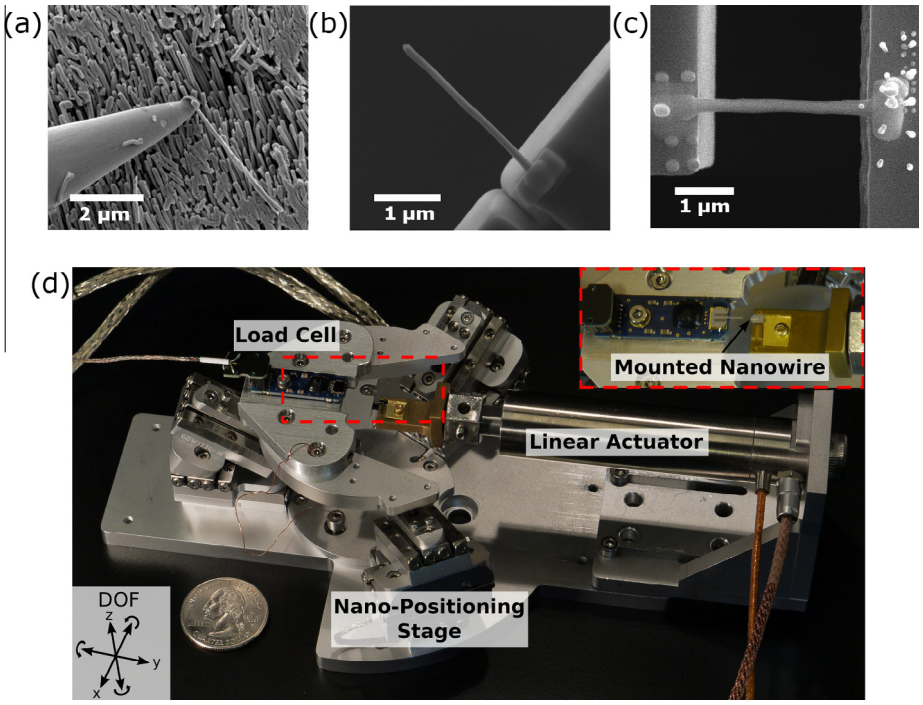

Fig. 1. (a) Example of a nanowire being harvested. (b) A harvested nanowire mounted on a prepared AFM cantilever using Pt-EBID. (c) A nanowire gripped at both ends and ready for tensile testing. (d) The nanomechanical testing platform, with the translational and rotational degrees for freedom indicated; a quarter is shown for scale. The inset shows an expanded view of the load cell and sample mount.

To perform a tensile test, the sample was placed on the linear actuator and aligned with the load cell using the 6 DOF stage. The wire was secured to the load cell using the Pt-based EBID. The nanowire was then strained at a nominal strain rate of $5 \times 10^{-4}\ s^{-1}$ while simultaneously recording the load and images of the test. After testing, digital image correlation (DIC) was used to extract strain measurements from the image sequences. Markers placed on the grips were tracked to determine the strain [66,67].

Nanowires were irradiated under a variety of conditions in a dual-beam SEM/FIB to vary the irradiated volume fraction and ion fluence. The irradiated volume fraction was controlled by changing the Ga^+ accelerating voltage of the FIB. To this end, accelerating voltages of 5, 15 and 30 kV were used. Stopping range of ion calculations (SRIM.org) were performed to determine the ion range and damage distribution at each accelerating voltage. Each simulation used 10,000 ions and full damage cascades were calculated. Fig. 2c–e shows the calculated ion range and damage distributions, as well as the irradiated volume fraction calculated using an assumed damage cross-section shown in Fig. 2b. The ion stopping ranges were calculated to be 2.4, 4.7 and 7.6 nm for 5, 15 and 30 kV, respectively. To irradiate a nanowire, the electron and ion beams were aligned well away from the sample to ensure that the beams were focused at the same point with the electron beam perpendicular to the nanowire. The sample was then located using the electron beam, and a reduced scan was placed on the gage length such that approximately 1 μm was exposed. Using a low beam current (10–30 pA), the ion beam was rastered over the nanowire a controlled number of times. This process is shown schematically in Fig. 2a.

The experimental ion fluence (f) was calculated according to

$$f = \frac{INt}{qA_{pxl}n_{pxl}} \tag{1}$$

where I is the ion beam current, N is the number of times the ion beam was rastered over the sample, t is the ion beam dwell time, q is the elemental ion charge (i.e. for Ga^+ $q = 1$), A_{pxl} is the real area of a pixel and n_{pxl} is the number of pixels. As a result, the ion fluence was controlled by varying the number of times the ion beam was rastered over the sample. Ion fluences ranging from 0 ions/nm^2 to $\sim$ 300 ions/nm^2 were used. These values were determined based upon the Ga ion current measured by a Faraday cup in the ion column at the time of each experiment and monitored during the irradiation process, which showed that the standard deviation of the beam current had an upper limit of 1 pA. In addition, the effect of structural relaxation annealing on irradiated wires was considered. Selected nanowires were irradiated with fluences between 115 and 145 ions nm^{-2} and subsequently annealed at $0.96T_g$ for 70 min – conditions we previously showed to reverse the effect of ion irradiation on deformation mode [54].

Irradiated nanowires were characterized by selected area electron diffraction (SAED) to confirm the amorphous structure. Wires were mounted to transmission electron microscope (TEM) lift-out grids to eliminate possible

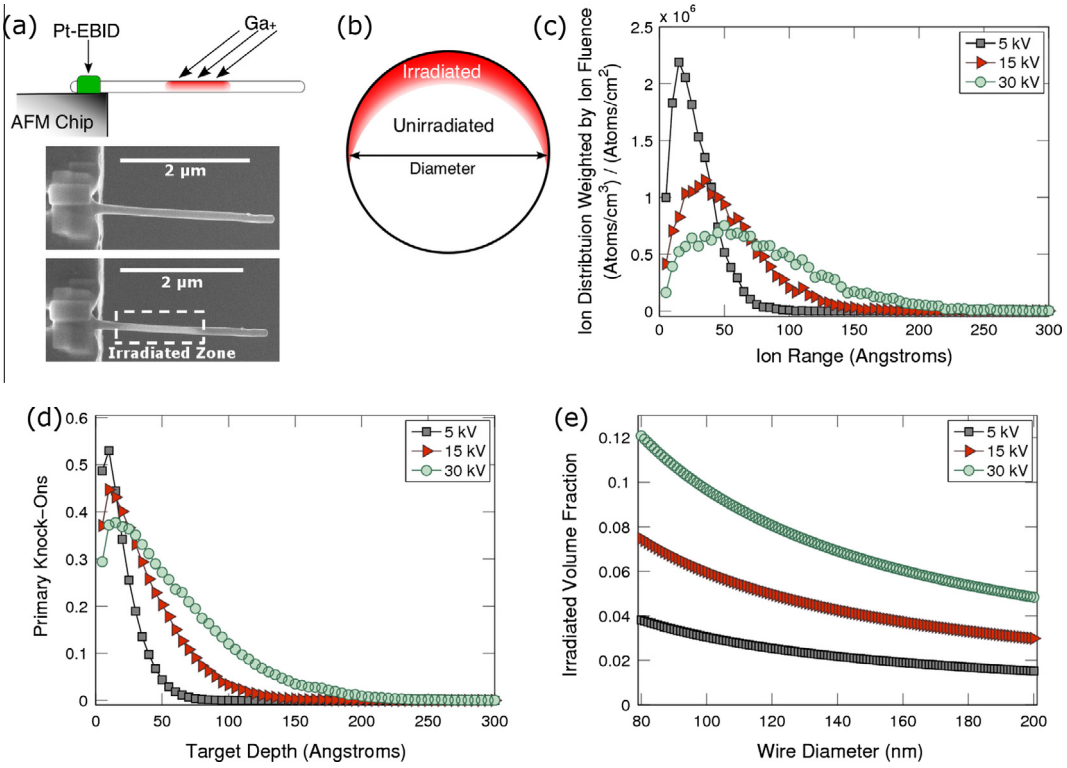

Fig. 2. (a) A schematic of the nanowire irradiation process. In the dual-beam SEM/FIB a portion of the gage length is irradiated by a beam with an incidence angle of 38° with respect to the nanowire axis. The assumed cross-section used to calculate the irradiated volume fraction is illustrated in (b). The red region represents the irradiated material and the white area indicates the unirradiated volume. Results of ion stopping range calculations showing (c) the ion implantation range and (d) the distribution of primary knock-on damage. (e) The calculated irradiated volume fraction for each accelerating voltage. (For interpretation of the references to color in this figure legend, the reader is referred to the web version of this article.)

background from carbon grids, using the same harvesting process that was used to prepare the tensile specimens. Diffraction patterns were obtained using a JEOL 2100 TEM with an accelerating voltage of 200 keV. Using SAED, a central portion of the nanowire was selected such that the lift-out grid and Pt-EBID did not contribute to the diffraction pattern. To analyze the diffraction patterns, the radial intensities were integrated. The limits of integration were selected to avoid contributions from the beam stop, and the same limits of integration were used for all diffraction patterns.

Atom probe tomography was used to quantify the Ga content in both irradiated and as-molded nanowires. In the atom probe, the nanowire is subjected to a high electric field, which is used to ionize and remove single atoms from the surface, which are then captured on a 2-D detector and identified by their time-of-flight. This allows for precise compositional analysis of very small volumes of material. For this purpose, nanowires were manipulated via the same methods used to prepare wires for tensile testing and welded with Pt-based EBID onto a support structure for analysis [68]. The ends of the nanowires, which often showed structural irregularities, were cut off using a Ga FIB with an energy of 30 keV. As the atom probe data set was collected from this near-tip region, this implied that the Ga content measured systematically represented the upper limit of the actual Ga composition in tensile specimens. After processing in the FIB, some wires were then annealed before atom probe analysis under the same conditions used to structurally relax wires for tensile testing. The atom probe experiments were carried out in a Cameca LEAP 4000× Si instrument using 90 pJ laser pulses to trigger the field evaporation. The base temperature used was 60 K.

3. Experimental results

3.1. Structural characterization

To verify that the nanowires remained fully amorphous and to attempt observations of changes in structure, irradiated wires are examined using a TEM. Fig. 3 shows diffraction patterns of as-molded nanowires and irradiated nanowires for two different ion fluences. No crystal diffraction spots are observed in the unirradiated or irradiated diffraction patterns, indicating an amorphous structure. However, subtle changes in the second diffuse scattering ring are observed. The integrated intensities and corresponding difference curves (Fig. 3e and f) show that the wires irradiated at 123 and 221 ions nm^{-2} undergo a structural change which induces a detectable change in the second ring. Before irradiation, the second diffraction ring is relatively broad (Fig. 3c) and shows signs of splitting, as evidenced by the integrated intensities (Fig. 3e and f). After

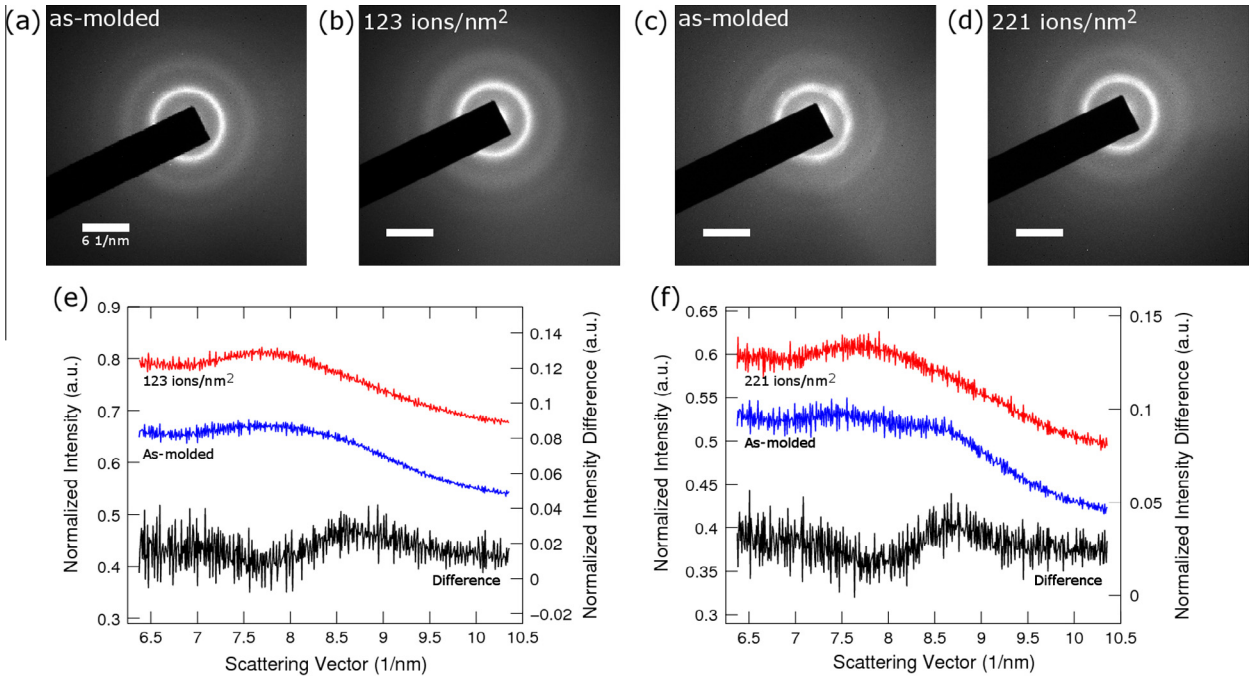

Fig. 3. Selected-area transmission electron microscopy diffraction patterns of nanowires irradiated at different ion fluences. (a and c) Diffraction patterns from two individual wires before irradiating. (b) A diffraction pattern of the wire in (a) after irradiation at 123 ions nm^{-2}. (d) A diffraction pattern of the wire in (c) after irradiation at 221 ions nm^{-2}. In all patterns, no obvious crystal diffraction spots are observed. (e and f) Integrated intensity profiles of the second peak for patterns (a) & (b) and (c) & (d), respectively, with the difference between the two patterns shown. The intensities are normalized by the intensity of the first peak and offset for clarity.

irradiation, peak splitting is no longer detectable in the second diffraction ring. This subtle change may be indicative of changes in the mid-range order and points to a more liquid-like structure, as corroborated by recent molecular dynamics (MD) simulations showing reductions of icosahedral cluster populations owing to ion irradiation [49], though systematic quantification proved challenging.

Results from atom probe analysis of nanowires in the as-molded state give a composition of $Pt_{56.0}Cu_{16.7}Ni_{7.3}P_{20.0}$, which agrees very well with the composition of the starting MG materials, confirming that the molding process does not significantly alter the composition of the resulting nanowires. Analysis from both the irradiated and irradiated plus annealed states indicate that there is a measurable decrease in Ga content beneath the surface of the wires after annealing. For the volumes analyzed, the total amount of Ga found 15–30 nm below the surface was 2.0 ± 0.4 at.% before and 0.25 ± 0.05 at.% after annealing. As previously discussed, these values represent the upper limits of the Ga concentration (relative to irradiated tensile specimens) owing to the preparation of atom probe tips. The ends of the wires prepared for the atom probe had been trimmed with the 30 kV ion beam, thus the ion implantation profile was expected to be close to equilibrium [69]. However, since the exact equilibrium shape was unknown, we could not quantify the precise Ga dose or account for variations in dose from wire to wire due to differences in sample preparation. Therefore it was not possible to precisely quantify the reduction in Ga concentration for the nanowires used for mechanical testing. Nevertheless, we were able to qualitatively confirm that the Ga concentration in the sub-surface regions is reduced after annealing.

3.2. Tensile response of irradiated nanowires

Whereas any major structural changes are virtually undetectable by the scattering methods used here and the extent of Ga incorporation was shown to be minimal, the amorphous structure was retained following all ion irradiation treatments, and clear changes in mechanical response were measured as a function of the different irradiation treatments. Fig. 4 shows representative stress–strain curves of MG nanowires irradiated at 5 and 30 kV for diameters ranging from 100 to 160 nm. We first describe our reference behavior, which is that of the as-molded nanowire, which shows linear elastic loading followed by abrupt failure. This is characteristic of metallic glasses tested in tension at room temperature [2]. In contrast, the irradiated nanowires show an increasing amount of plastic strain and a decreasing apparent yield stress (defined as the stress at which the response clearly deviates from linear elasticity) as the ion fluence is increased. These general trends appear to be relatively insensitive to the ion accelerating voltage (and thus the irradiated volume fraction), as shown for the stress–strain curves corresponding to 5 kV (Fig. 4) and 30 kV (Fig. 4b). We note that the appearance of inelasticity occurs at relatively low ion fluence levels ($\sim$30 ions nm^{-2}) for both accelerating voltages. The nanowires irradiated at 30 kV (and to a lesser extent those

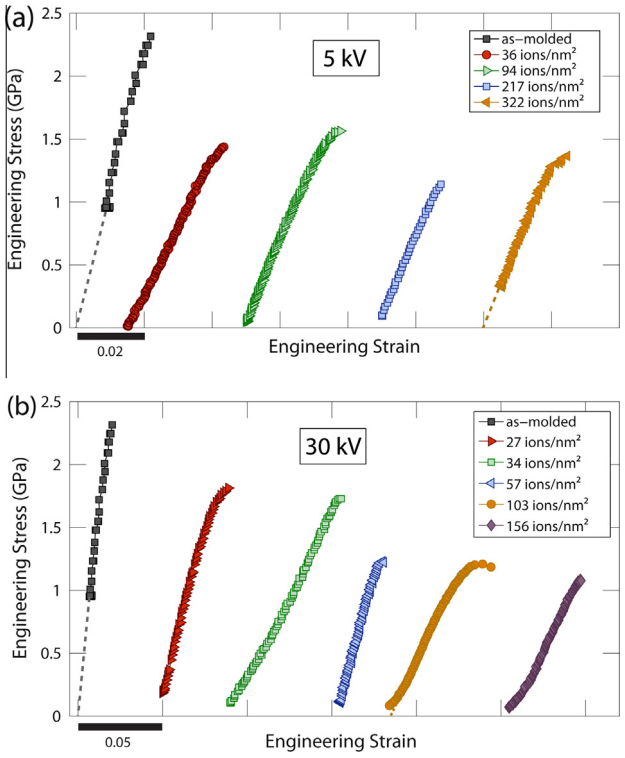

Fig. 4. Representative stress–strain curves for nanowires irradiated at (a) 5 kV and (b) 30 kV, with increasing ion fluences.

irradiated at 5 kV) show significant scatter in the apparent Young's moduli, which we attribute to the compliance of the gripping materials that contributes to the measured strain [67]. While the DIC techniques used to measure strain yield a noise floor ($\Delta\varepsilon$) of $\sim 4 \times 10^{-4}$, the strain is measured from markers placed on the grips. Thus the strain measured is the total strain in the nanowire-EBID grip system. Using the elastic modulus of the bulk [23], we estimate the nanowire stiffness to be within an order of magnitude of the EBID grip stiffness. Therefore, the uncertainty in any modulus measurement is roughly 10–20% from the grip compliance alone [67]. This uncertainty is typically greater than that due to other factors (i.e. force and cross-section measurement), and is much higher than the expected change in modulus due to modification of the glass structural state [25]. Thus, despite the reported correlation between glass structure and elastic modulus that supports our observations of lower modulus with increasing ion damage, the resolution and scatter of our elastic modulus measurements prove inconclusive.

3.3. Effect of ion irradiation on tensile ductility and yield strength

To systematically demonstrate the effect of ion fluence and irradiated volume fraction on the amount of plastic deformation observed, we compile a deformation mechanisms map showing both the plastic strain normalized by the total strain to failure (color) and the failure mode as a function of ion fluence and irradiated volume fraction (Fig. 5a). In the map, the triangles indicate failure characterized by shear banding, the circles indicate wires the deformation of which was characterized as ductile (quasi-homogeneous) and the diamonds indicate nanowires which failed in a mode that was neither a shear band nor ductile, which we describe as "intermediate". The type of deformation is determined based on the force–time curves and images of the fracture surface that showed a diversity of morphologies, as shown in Fig. 5b–d. Representative and normalized force–time curves are shown alongside corresponding fracture morphologies to facilitate comparison between the different deformation modes. The brittle-like mode with signature shear-band-mediated failure is characterized by a force–time curve with a constant slope up until failure (black curve in Fig. 5) and a sharp-angled fracture surface indicative of a shear band. In contrast, the ductile-like mode is indicated by a clear change in slope of the force–time curve (yellow curve in Fig. 5d) before failure and a fracture surface that shows clear evidence of plastic deformation (e.g. rounding of the fractured edges). The "intermediate" mode is characterized by a less distinct change in slope of the force–time curve (as indicated by the deviation of the red curve in Fig. 5c from the dashed blue line) and fracture surfaces that cannot clearly be delineated as shear band mediated or ductile; rather, they show signatures of both behavior simultaneously.

The deformation map for plastic strain shows two trends. First, there is a clear trend in the mode of deformation (indicated by the data marker symbol type in Fig. 5). At low ion fluence and irradiated volume fraction, the deformation mode is characterized as shear band mediated, similar to the as-molded case. At high ion fluences and irradiated volume fractions, the deformation mode is characterized as ductile. Between the shear band and ductile regimes an intermediate regime is observed. Some plastic deformation is detected in this region, but the fracture surface is not clearly a shear band or ductile mode. The dashed lines in Fig. 5 show the transition between the deformation modes.

The other trend apparent in our data is a general increase in the amount of plastic deformation with increasing ion fluence and irradiated volume fraction. The correlation between plastic strain and ion irradiation conditions is not as pronounced as in the transition in deformation mode. Some nanowires characterized as intermediate showed more plastic deformation than nanowires characterized as ductile. These observations suggest that the extent of ductility in a glass, much like that in crystalline materials, is not a deterministic parameter but instead is governed by the stochastic nature of local inelastic rearrangements (e.g. STZs) and the evolution of plastic damage in disordered materials.

Similar to the amount of measured plastic deformation, the decrease in yield stress shows a trend with ion fluence and irradiated volume fraction, as shown in the yield stress deformation map of Fig. 6. At low ion fluence and irradiated volume fraction, the yield stress is similar to

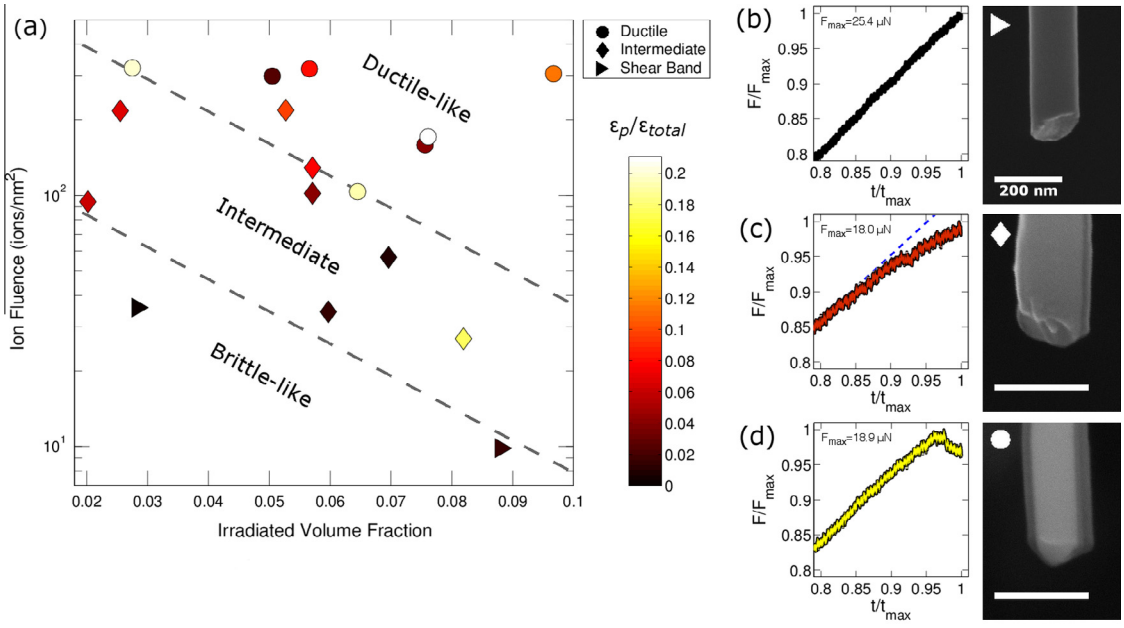

Fig. 5. (a) Deformation map showing the influence of ion fluence and irradiated volume fraction on the amount of plastic strain. The plastic strain is normalized by the total strain to account for differences in grip compliance. The dashed lines are to guide the eye to the transition between deformation regimes. (b–d) Typical force–time curves and fracture morphologies for the shear band, intermediate and ductile-type deformation, respectively. The force–time curves are normalized by the maximum force, which is indicated on the plot, and time at failure in order to facilitate comparison of the different deformation modes. The colors of the curves match the color scale of (a), marking the approximate extent of plastic strain. (For interpretation of the references to color in this figure legend, the reader is referred to the web version of this article.)

the previously reported mean yield stress of 1.6 GPa for the as-molded Pt-glass nanowires [54]. As the ion fluence and irradiated volume fraction increase, a decrease in yield stress is observed. To determine the predominant factor – irradiated volume fraction or ion fluence – linked to changes in yield stress, we examined the correlations individually, as shown in Fig. 6b and c. The plot of yield stress vs. irradiated volume fraction (Fig. 6b) shows no clear correlation in the range of volume fractions sampled. The plot of yield stress vs. ion fluence (Fig. 6c), however, shows a trend towards decreasing yield stress with increasing ion fluence. A linear fit is shown in Fig. 6c to emphasize the trend towards lower strength. In addition, the linear fit shows good agreement with the as-molded strength. From these analyses, it is clear that ion fluence (thus, extent of displacement damage) plays the dominant role in changing glass structure and concomitant mechanical behavior in our study despite the difference in ion energies (and hence range). The importance of extent of damage is further bolstered by measurements of the tensile behavior of ion-irradiated nanowires subsequently subjected to structural relaxation annealing. Five irradiated wires, subjected to ion fluences between 115 and 145 ions/nm^2, were administered structural relaxation annealing before measuring the tensile response. The yield strength of the irradiated and annealed samples returned to the as-molded level or even higher, as shown by the open symbols in Fig. 6c.

In order to highlight the differences in glass structure and the corresponding effect on strength more clearly, we also show the measured strength grouped by treatment in Fig. 7. In Fig. 7, the average strength of the as-molded, heavily irradiated, and irradiated and subsequently annealed samples are shown as a bar, with an error bar corresponding to the standard deviation of the group. Here the heavily irradiated condition is considered to be the top third of the ion fluences used, which corresponds to ion fluences greater than 200 ions/nm^2. As previously reported, the as-molded nanowires showed a mean yield strength of 1.6 ± 0.4 [54]. The mean yield strength and standard deviation of the heavily irradiated and irradiated then annealed groups are 1.25 ± 0.2 and 1.8 ± 0.26 GPa, respectively. This strongly indicates that the behavior of the heavily irradiated samples is distinctly different from that of the as-molded and irradiated then annealed samples. We note that the apparent trend in strength as a function of ion fluence contains a stochastic character, which is presumably due to the probabilistic nature of the ion collision cascade process. Indeed, atomistic simulations on ion-irradiated metallic glasses [49] suggest a more deterministic relationship between yield strength and potential energy per atom, which is unfortunately not easily measured in our experiments.

The insensitivity to the irradiated volume fraction over the range studied can be reconciled by considering the distribution of damage created by ions at different accelerating voltages. Despite the different damage distributions, the peak damage occurred within 5 nm of the surface irrespective of ion accelerating voltage (Fig. 2c). Nevertheless, it is interesting to note that substantial differences in mechanical behavior can be detected even with irradiated volume fractions as small as 2%. Taken as a whole, the yield strength changes measured as a result of ion irradiation (decreasing

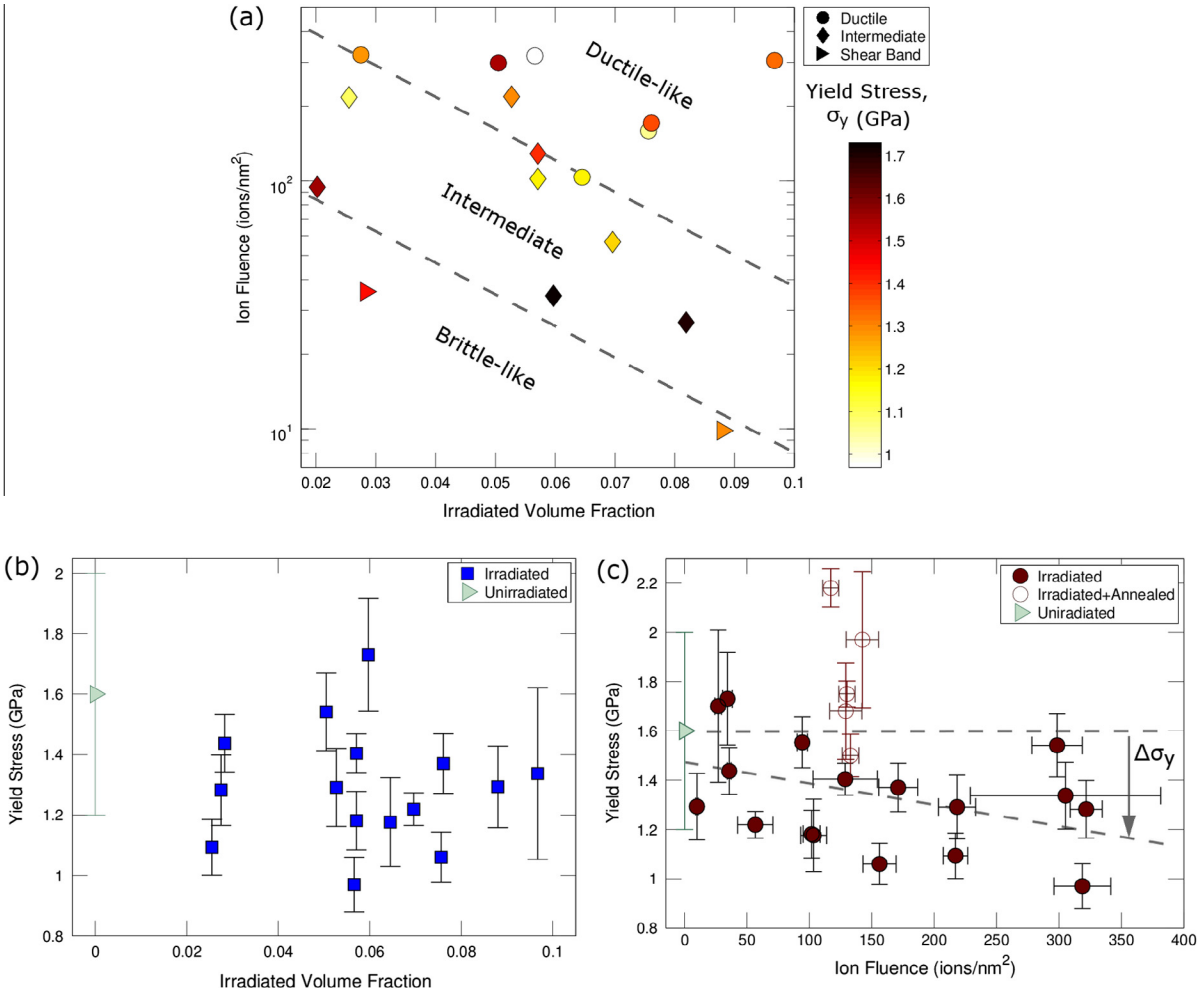

Fig. 6. (a) Deformation map showing the influence of ion fluence and irradiated volume fraction on yield stress. The dashed lines are to guide the eye to the transition between deformation regimes. (b) Yield stress plotted vs. irradiated volume fraction. No clear trend with irradiated volume fraction is observed. (c) Yield stress as a function of ion fluence. The average yield stress of the as-cast nanowires is indicated by the green triangle. Closed circles represent irradiated nanowires while open circles represent irradiated nanowires subjected to a relaxation anneal. Yield stress appears to decrease with increasing ion fluence and this trend is emphasized by a linear fit to the data. The horizontal line indicates the as-molded yield stress and the sloped line is the linear fit which agrees well with the as-molded yield stress. The error bars for the unirradiated state in (b) and (c) are the standard deviation of 10 tensile tests, while those for the irradiated and irradiate + annealed states are estimated errors based on experimental uncertainty. Error estimates for ion fluence are also included in (c) based on the measured ion beam current standard deviation of 1 pA. (For interpretation of the references to color in this figure legend, the reader is referred to the web version of this article.)

strength) and subsequent annealing (increasing strength) suggest the ability of our treatments to strongly modify the glass structure so as to manifest as substantial changes in the plastic behavior of our nanowires. In the sections that follow, we discuss this correlation between glass structure and mechanical strength and propose a universal model capable of predicting the yield strength of a metallic glass across a wide range of structural states.

4. Discussion

4.1. Size-independent transition in plastic deformation owing to ion irradiation

To explain the observed changes in mechanical behavior of our MG nanowires, we consider glass parameters that could contribute to our experimentally measured increases in ductility and decreases in yield stress. Possible factors include changes in structure, chemistry, free volume and the corresponding elastic constants. However, detecting site-specific structural changes in our nanowires through electron diffraction have proven to be elusive due to limited resolution. Measuring changes in free volume in an irradiated nanowire would be similarly challenging. Free volume is often directly measured through positron annihilation spectroscopy. However, the high energies and large spot sizes are mainly suited for probing bulk structures and not single nanowires [70]. Other possible metrics for evaluating irradiation-induced changes in the glass are the elastic properties. While a high Poisson's ratio (or low μ/B) is often associated with more ductile metallic glasses, recent work by Kumar et al. has shown the elastic properties to be insensitive to different structural states, as evidenced by measurements of fictive temperature T_f [25,26,31].

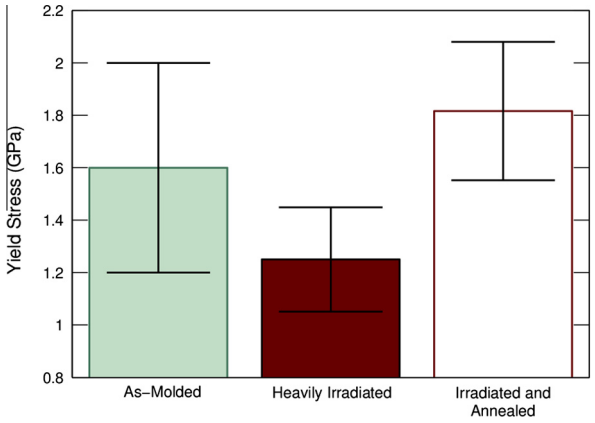

Fig. 7. Direct comparison of the effect of different Ga ion treatments on the average measured strength. Here the as-molded strength (1.6 GPa) is directly compared to the highest third of ion fluences employed (1.25 GPa) and the irradiated and subsequently annealed treatments (1.8 GPa). The error bars are the standard deviation of each treatment group. This comparison emphasizes the significant decrease in strength due to ion irradiation and the subsequent recovery due to relaxation annealing.

However, glasses prepared in different structural states show a transition from brittle to extended plastic behavior, casting doubt on the use of Poisson's ratio alone as a predictive metric for ductility. Furthermore, the changes in elastic properties demonstrated by Kumar et al. are small compared to the resolution of our nanoscale experiments [25,31]. We thus focus our attention on other glass parameters with known sensitivity to glass processing and, correspondingly, structural state, which may explain the dramatic changes in plastic response that we have measured.

4.2. Revisiting kinetic and thermal phenomena in amorphous materials below the glass transition

We consider kinetic and thermodynamic physical properties of MGs, namely, glass transition and fictive temperatures, respectively, as descriptors of structural state and thus changes in mechanical behavior. We begin our discussion by briefly reviewing the conceptual notions and experimental considerations that underlie the use of glass transition and fictive temperatures to connect to inelastic mechanical behavior. The glass transition is a kinetic phenomenon [71,72]. As the liquid is quenched (or the solid is heated), a temperature – the glass transition temperature – is reached at which structural relaxation times are on the order of ~ 100 s as the material changes from a supercooled liquid to a kinetically frozen glass (or vice versa) [71,73]. Measurements of T_g are often performed using calorimetric means, with T_g depending on the cooling or heating rate used to make the measurement. Higher cooling rates result in higher T_gs, but orders of magnitude changes in rate produce relatively small changes in T_g [74]. However, asymmetric cooling and heating (i.e. cooling faster than heating) results in a different measured T_g on heating vs. cooling. As a result, to obtain a consistent and reproducible T_g, the glass should be cooled and heated at the same rate and as close to equilibrium as possible while still avoiding crystallization [71]. For experimental practicality, within the metallic glass community T_g is typically reported on heating at approximately 20 K/min.

In addition to the effect of cooling rate, small changes in T_g can be induced through processing treatments such as annealing. For instance, changes in the glass transition due to aging of an MG can be measured [75–77]. Aging an MG at temperatures below T_g has been shown to relax the structure, reducing the free energy and free volume. Changes to T_g due to aging are typically less than 10 K even for complete relaxation of the glass, although the amount varies for different glass compositions [75–77]. Mechanical treatments such as severe plastic deformation have also been reported to have little effect on T_g despite reports of large changes in hardness, elastic modulus and calorimetrically measured exothermic peaks prior to the glass transition [41,42].

Whereas T_g is insensitive to cooling rate, annealing and severe plastic deformation treatment, T_f can vary widely [78–81]. In contrast to T_g, the fictive temperature is a thermodynamic variable describing the temperature at which the kinetically frozen structure is at equilibrium with the liquid [32], and is qualitatively related to structural descriptors like free volume [72]. A given fictive temperature does not specify a unique glass structure; rather, many possible structures may result in the same observed fictive temperature [82]. Importantly, T_f can be greater than or less than T_g, and varies semi-independently of T_g. While T_g typically changes by less than 10 K for a fully relaxed glass, the fictive temperature has been observed to change by more than 20 K for shorter relaxation times [80]. Hyperquenching oxide glasses has also resulted in glasses with a T_f as high as 1.22 T_g, yet T_g was reported to change little after relaxing the quenched glass [79]. Finally, the large excess enthalpies observed in glasses subjected to HPT indicate a high fictive temperature, yet T_g was observed to be invariant [41,42]. These results collectively point to T_f as a much more sensitive predictor of the structural state of a given glass, as supported by systematic calorimetric measurements in the literature [83,84], which suggests a correlation between T_f and the concentration of flow defects [84]. In the discussions and analysis that follow, we assume T_g to be relatively constant for our metallic glass experiments and attribute the observed change in material response owing to ion irradiation and subsequent structural relaxation annealing to changes in structural state as reflected in T_f.

4.3. Correlations between T_f and plastic deformation, and T_g and yield strength

We next examine correlations between the thermodynamic and kinetic properties of a metallic glass with its mechanical behavior. A recent report by Kumar et al. showed that increasing T_f in several MGs increased the capacity for plastic deformation in bending [31]. Thus,

the increase in plastic deformation that we measured could similarly be justified through an increase in T_f due to ion irradiation. Analogously, the increase in tensile ductility could be attributed to an increase in liquid-like states or higher free volume [85,86]. In the case of yield strength, the observed changes could be rationalized through changes in T_g, as recently proposed. Yang et al. and Liu et al. reported unified predictions of yield stress entirely as a function of a given MG's molar volume and $T_g - T_o$, where $T_o \ll T_g$ is the testing temperature (the details of this prediction will be presented in greater detail in the following analysis) [87,88]. Briefly, a glass with a higher T_g or lower molar volume would be expected to exhibit a higher yield strength (and elastic modulus). Based on this prediction, we can examine the effect that irradiation has on the expected change in yield strength of our MG nanowires. Assuming that irradiation effectively shifts our MG along Yang et al.'s universal scaling curve, our measured reductions in yield stress owing to ion irradiation would indicate a decrease in T_g of ~ 40 K (changes in molar volume are estimated to be negligible). Such a reduction of T_g estimated by this yield stress prediction is the opposite of what one would expect for a more ductile glass. Rather, a reduction of T_g indicates a more relaxed glass state (analogous to a relatively slow cooling rate), which would be expected to be more brittle in comparison to the as-molded condition. This failing of the unified strength scaling to describe our experimental results suggests that the structural state of a given MG system is not described by this relationship. Thus, in order to properly account for the observed changes in ductility and yield stress, we propose the incorporation of a structural state descriptor given by T_f, which can capture the processing dependence of a given MG.

4.4. New analytical model for universal strength scaling dependent on glass structural state

To understand the influence of T_g and T_f on yield strength, we begin by revisiting the universal MG yield strength predictions presented by Yang et al. [87] and Liu et al. [88]. Both models are predicated on equating the change in internal energy as a glass is taken through the glass transition into the supercooled liquid regime to the work performed to initiate a mature shear band. Mechanistically, this equality is rooted in the similar structural signatures associated with local plastic shearing and the glass transition, with dilation and free volume production occurring in both cases, as quantified by decreases in viscosity. Two analytical models have been proposed that result in the same scaling but with subtly different approaches, with Yang et al.'s prediction [87] implicitly assuming a free volume-mediated mechanism to formulate their theory. Liu et al. [88], on the other hand, developed their model on simple thermodynamics without recourse to an assumed deformation mechanism. Despite these differences, the net results and scaling behavior are equivalent as the latter model recovers the former.

Liu et al. assumed the plastic yield process to be volume preserving. Thus the work done can be written as $dW = V_s\gamma_0 d\tau$, where V_s is the volume undergoing a transition due to plastic flow, γ_0 is the critical strain for shear instability and τ is the applied shear stress [88]. Furthermore, for a constant volume system, the change in internal energy can be written as $dU = \rho V_s C_v dT$. By assuming that the heat released during yield is much less than the work done by the applied stress (i.e. $dQ \ll dW$), an expression was derived equating the work done to changes in internal energy (Eq. (2)) [88].

$$V_s\gamma_0 \int_0^{\tau_y} d\tau = V_s \int_{T_o \ll T_g}^{T_g} \rho C_v dT \tag{2}$$

The integration bounds represent a transit through the yield point and, equivalently, from room temperature (T_o) through the glass transition.

While Liu et al. assumed the Dulong–Petit limit of heat capacity, Yang et al. adopted the Debye model for heat capacity [87,88]. By integrating the Debye heat capacity, the yield stress was related to the glass molar volume and T_g as

$$\sigma_y \approx \frac{6Nk(T_g - T_0)}{\gamma_0 V} \tag{3}$$

where N is Avagadro's number, k is Boltzman's constant, γ_0 is the shear disordering strain, which is assumed to be of order unity, and V is the molar volume. This scaling of yield strength is equivalent to Liu et al.'s prediction [88]. Such universal scaling between stress and temperature (and thus viscosity) in an MG and the physics underlying a stress-induced glass transition is also supported by MD simulations of a Zr-based MG [89].

However, we observe that this prediction does not account for the state in which the glass is kinetically frozen, which would suggest that a given glass's yield strength and capacity for plastic flow at a given temperature are insensitive to the processing route and thermomechanical history. This is in stark contrast to experimental evidence, including ours, showing substantial changes in strength and hardness of a given MG system in different structural states [40,44,46,90]. In fact, if we assume the maximum change in T_g to be ~ 10 K, as measured previously in other glass systems [75–77], we find that the predicted yield stress would change by only ~ 70 MPa, which is inconsistent with our results. Therefore, we propose a revised model, which explicitly accounts for the wide structural spectrum in which a given MG can exist. Glasses are well known to store excess enthalpy, with the magnitude of such enthalpy depending on the cooling rate, aging/rejuvenation annealing treatments [91] and degree of severe plastic deformation [42]. Therefore, by noting that the T_g used as an integration bound is measured via the consistent measurement method (and is therefore constant), we include an

additional term representing the excess enthalpy with respect to a known reference state, such as the as-quenched glass, normalized by the molar volume. This excess enthalpy allows glasses prepared in different states to be distinguished – a feature not captured in previous unified strength models. Accordingly, we propose a new yield prediction:

$$\sigma_y \approx \frac{6Nk}{\gamma_0 V}\left(T_g - T_0\right) - \frac{\Delta H_{g-g'}}{V} \tag{4}$$

where $\Delta H_{g-g'}$ is the excess enthalpy with respect to a glass reference state such as the as-quenched glass (g'). The presence of such excess enthalpy would add to the stored elastic energy during deformation, which is consequently balanced by the internal energy of the system, and thus could be considered as an excess defect energy. In our experiments, the defect energy would be incorporated via ion irradiation-induced changes in the glass structure and could be reduced through subsequent structural relaxation annealing as we have performed.

To compare with experimentally tractable properties, we relate this additional excess enthalpy term to T_f by considering the measurement and analysis of T_f. From Moynihan et al. [78], T_f is determined according to

$$\int_{T'}^{T_{eq}} \left(C_p - C_{pg}\right) dT = \int_{T_f}^{T_{eq}} \left(C_{pl} - C_{pg}\right) dT \tag{5}$$

where C_p is the measured heat capacity, C_{pg} is the equilibrium glass heat capacity extrapolated to high temperatures, C_{pl} is the equilibrium liquid heat capacity extrapolated to low temperatures, T' is any temperature well below the glass transition and T_{eq} is any temperature well above the glass transition where the heat capacity has reached its equilibrium liquid value. To obtain an expression for T_f, we adapt the method described by Yue et al. [79], where the left-hand side of Eq. (5) is simply the enthalpy difference between the glass state at T' and the liquid state at T_{eq} $\left(\Delta H_{l-g}\right)$. From Adams and Gibbs [92], $C_{pl} - C_{pg}$ is assumed to be constant close to the glass transition. Indeed, if we consider the heat capacity difference for the Pt-glass used, $C_{pl} - C_{pg}$ varies by less than 30% over $T_g \pm 50$ K [93]. Therefore a simple expression to estimate T_f can be developed by integrating the right-hand side of Eq. (5) and solving for T_f (Eq. (6)). Since ΔH_{l-g} is a measurable quantity, T_f can be estimated from calorimetric measurements.

$$T_f = \frac{-\Delta H_{l-g}}{C_{pl} - C_{pg}} + T_{eq} \tag{6}$$

Next, we consider two glasses prepared in different states, denoted a and b. The two glasses therefore have distinct values of $\Delta H_{g-g'}$ and ΔH_{l-g}, and consequently the difference in T_f between the two states can be related to the enthalpy difference of the two states as given by

$$\Delta T_f = \frac{\Delta H_{a-b}}{C_{pl} - C_{pg}} \tag{7}$$

Taking the difference in yield stress between two states provides the energy difference between the two states as Eq. (8):

$$\Delta\sigma_y = -\frac{\Delta H_{a-b}}{V} \tag{8}$$

Finally, Eqs. (7) and (8) are combined to relate the yield stress difference to a change in fictive temperature (Eq. (9)):

$$\Delta T_f = \frac{-\Delta\sigma_y V}{\left(C_{pl} - C_{pg}\right)} \tag{9}$$

Here, we have developed the relationship between T_f and yield stress based on the assumption that T_f changes to a much greater extent than T_g. However, it is important to note that this assumption is not central to the expressions developed, as it is similarly effective to begin with the observation that the unified yield stress models of Yang et al. and Liu et al. incorrectly predict changes in T_g. Indeed, one could simply add the excess enthalpy term to Eq. (4), where the T_g term is taken to be a known reference state. In this case, the as-quenched glass state would be the appropriate choice, and subsequently the fictive temperature changes could be introduced again using the as-quenched state as the reference. Finally, by equating the enthalpy differences, we recover Eq. (9) without considering the relationship between T_g and T_f, but instead simply comparing all yield stresses and T_f to a known reference state.

Using Eq. (9), the changes in T_f due to glass processing (in our experiments, ion irradiation) can be estimated from changes in yield stress. From Fig. 7, the yield stress decrease is approximately $\Delta\sigma_y = -350$ MPa, based upon the processing groups. The heat capacity difference is estimated to be 30.6 J/mol K at T_g [93], and V is calculated based on a linear rule of mixtures to be 8.76 cm^3/mol [23]. The resulting maximum change in fictive temperature is thus ~ 100 K or $0.2T_g$. Achieving such changes in T_f through cooling rate variation in a typical MG would require rates approximately ten orders of magnitude higher than for the standard as-cast state [94]. Taken as a whole, our experimental measurements of yield strength changes and modeling strongly suggest that ion irradiation dramatically influences the structural state of our glass by the incorporation of large defect energies (rejuvenation) that can be recovered via structural relaxation annealing treatments. This latter point also implies that any chemical changes to our MG nanowires as a result of ion implantation cannot, to first order, explain the large changes in mechanical behavior or their inherent reversibility.

To test the validity and robustness of our new model, we also applied our analytical formulation and analysis to HPT results from the literature, where both changes in hardness and excess enthalpy as a function of cumulative plastic deformation were reported [42]. Meng et al. performed HPT on a Zr-based glass and measured its hardness and elastic modulus via nanoindentation, correlating such changes to calorimetric measurements of relaxation

enthalpy as a function of number of rotations and subsequent relaxation annealing [42]. As the number of rotations increased, the hardness decreased from 6.1 GPa for the as-cast glass to 4.9 GPa for 50 rotations; concomitant changes in relaxation enthalpy were approximately 1960 J/mol. Furthermore, HPT induced a change in indent morphology. In the as-cast state, clear shear bands were observed around the indent. As the number of rotations increased, a decrease in shear banding was observed. At 50 rotations, no shear bands were observed. Additional samples subjected to 50 rotations were annealed at 0.97 T_g for 1 h, which recovered the as-cast hardness, elastic modulus and indent morphology. As a whole, these HPT experiments show remarkable similarity to the ion irradiation experiments presented here in terms of the trends in yield stress, deformation behavior and reversibility, making the HPT results an apt test bed for the yield stress model presented here.

To apply our analytical model, we estimate the yield strength to be one-third the hardness [95]. We then apply Eq. (8) to estimate the energy difference between the as-cast and HPT (50 rotations) samples. The yield stress decrease is estimated to be −400 MPa for 50 rotations, which indicates an energy change of 4600 J/mol according to our model. From Eq. (7), and substituting ΔH, we then estimate ΔT_f to be 154 K. Based on the experimentally measured enthalpy relaxation, ΔT_f is estimated to be 65 K and $\Delta\sigma$ is estimated to be −170 MPa. Finally, structural relaxation annealing following HPT treatments recovered the hardness values of the as-cast MG.

Fig. 8a shows the experimentally measured [42] and calculated changes in yield stress as a function of number of HPT rotations (i.e. cumulative plastic strain), as well as the predicted yield stress from Yang's model [87]. The calculated annealed yield stress was determined by assuming complete relaxation (i.e. zero excess enthalpy in the system). In all cases, the approximated and calculated yield stresses are well below the predicted yield stress. Fig. 8b shows the changes in enthalpy and fictive temperature due to HPT determined using our newly developed analytical model. From these calculations we observe that the values determined from the hardness measurements are roughly three times greater than those estimated from the enthalpy relaxation measurements (Fig. 8b). We attribute this apparent discrepancy to the radially varying plastic strain inherent to the HPT disks; indeed, the center of the disk is less deformed than the edge. Thus, the enthalpy relaxation measurements probe the average change of the whole sample while the hardness measurements probe only a highly deformed region. However, the nominal shear strain gradient can be estimated as $\gamma = 2\pi Nr/t$ [39,41], where N is the number of rotations, r is the radial position and t is the thickness of the disk. The von Mises strain can then be estimated as $\varepsilon = \gamma/\sqrt{3}$ for small shear strains ($\lesssim 0.8$). However, in Meng et al.'s work, $\gamma \gg 0.8$ even for one rotation. As a result, an upper and a lower limit of accumulated strain will be considered. Two common strain estimates for materials subject to HPT are $\varepsilon = \left(\frac{2}{\sqrt{3}}\right) \ln\left[(1+\gamma^2/4)^{1/2} + \gamma/2\right]$ and $\varepsilon = \ln(\gamma)$, which we consider as an upper and a lower estimate of strain, respectively [43]. In light of the reported complexity of the strains incurred by HPT in polycrystalline materials, we note that the absence of microstructure and strain hardening mechanisms in metallic glasses greatly simplifies the picture and thus such modifications to the accumulated strain can be ignored. Then, by fitting the reported yield stress data as a function of number of rotations (and hence strain), the yield stress at each radius can be estimated. By applying Eqs. (8) and (7) and integrating over the disk radius, the total enthalpy and yield stress difference can be calculated. Fig. 8b shows the enthalpy and fictive temperature differences determined from the measured yield stress, calorimetric measurements and integrated estimate using the high

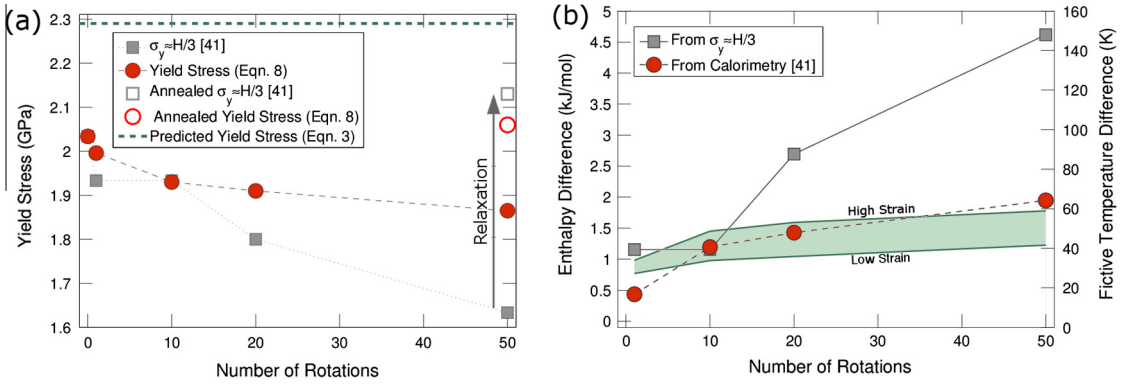

Fig. 8. HPT results [42] analyzed using the yield stress relationship to fictive temperature. (a) Changes in the yield stress (approximated as one-third of the hardness) determined from mechanical testing and calculated from the enthalpies of relaxation. The calculated yield stresses were determined using Eq. (8) using the as-cast glass as a reference state. The results after structural relaxation annealing (indicated by the arrow) are shown as open symbols. (b) The enthalpy difference between the HPT samples and the as-cast sample were determined from the approximated yield stress, directly measured by calorimetry and integrated from the yield stress assuming a linear relationship between the von Mises strain and yield stress. The green band is determined from the high- and low-strain estimates for HPT [43]; see the text for details. Enthalpy differences were calculated from Eq. (8) and fictive temperature changes were determined from Eq. (9). (For interpretation of the references to color in this figure legend, the reader is referred to the web version of this article.)

strain and low strain estimates as the upper and lower bounds, respectively. It is observed that the integrated estimate agrees well with the enthalpy difference as measured via calorimetry, providing additional validation of our model. This analysis thus shows that our revised model connecting plastic yielding in MGs is not only capable of describing strength differences between different glass systems, but can also successfully capture the continuum of structural states within a given glass system brought about by distinct treatments. We expect this approach to be applicable to various processing routes that either structurally relax or rejuvenate glasses.

4.5. Effect of Ga implantation on the observed mechanical response

From the atom probe results, it is clear that a non-negligible amount of Ga is incorporated in the nanowire during irradiation. In the irradiated wire, up to 2 at.% Ga was observed. However, it is important to note that this concentration was measured in the near-surface region, where the wire was cut using the FIB. As a result, this concentration may be taken as an approximate upper limit of Ga incorporation. However, dilute Ga will be incorporated into the nanowires at all fluence levels. Therefore, the possible effect of Ga on the mechanical properties is considered here.

Ga incorporation may alter the observed mechanical response through several mechanisms: induced residual stresses, compositional effects or the formation of a composite structure. Ion implantation leads to structural damage from collision cascades, but could also induce residual stress, with a gradient resulting from the ion range distribution. Recently the effect of residual stress on the observed mechanical response of MGs was studied via shot peening [44]. While shot peening could result in large compressive residual stresses at the surface, the measured yield stress was not significantly changed relative to unpeened samples. This contrasts with our results showing substantial and recoverable reductions in yield strength, which we thus ascribe to structural changes in the glass.

With regard to chemical shifts from ion implantation, results from the literature also suggest that small compositional changes should not significantly affect the properties of the Pt-based glass employed in this study [96]. Over a range of Pt compositions between 42.5 and 60 at.%, T_g and Vickers hardness showed only small changes of less than 3%. As a result, the substantial changes in both tensile ductility and yield strength measured in our irradiated nanowires are not commensurate with differences associated with the inclusion of small amounts of Ga and thus minor chemical shifts. The impact of residual stresses and composition is likely further diluted by the relatively small affected volume in the nanowire. In this work, the largest irradiated volume fraction was less than 10%. As a result, the majority of the nanowire is unaffected by irradiation, though the net mechanical response changes significantly.

Finally, it is conceivable that the irradiation process may create a composite structure consisting of a rejuvenated skin and a largely unaffected core. We believe that both our measured yield strength and the plastic deformation mode are largely controlled by the irradiated volume of the specimen, whereas the measurement of ductility is only weakly so. We hypothesize a mechanistic view of this as follows. First, ion irradiation clearly leads to softening of the material. Therefore the ion-damaged region is likely to commence yielding before the undamaged core, thereby controlling the measured yield point. Upon yield, the previously supported load is relaxed in the irradiated region due to plastic deformation and the majority of load bearing must now be borne by the core, which has a smaller cross-sectional area. Thus the stress rises rapidly in the core. Provided this increase in stress exceeds the elastic limit of the as-molded value, this event likely gives rise to yielding of the core, which follows in quick succession. As a result, we believe it reasonable to assume that our measurements of yield stress are predominately governed by the damaged zone of our irradiated specimens. This picture is supported by simulations of ion irradiation and mechanical properties in MGs [49], where ion collisions near the surface create a damage gradient from the surface to the core. This ion damage was also associated with a reduction in strength, in excellent agreement with our results.

In contrast, the quasi-isostrain configuration makes interpretation of ductility in such a composite structure complex. Plastic strain must be accommodated in both the rejuvenated skin and the unaffected core. Therefore, the achievable plastic strain is controlled by both regions. However, the undamaged core region is more susceptible to plastic instabilities or fracture, as shown by the brittle failure we observed in as-molded nanowires, which likely dominate the failure strain. Taken as a whole, we conclude that the measured changes from ion irradiation are primarily due to changes in the glassy structural state, as quantified by fictive temperature, and not due to stress or compositional effects.

5. Conclusions

Drawing connections between fundamental thermodynamic and physical parameters of glassy materials and their mechanical resistance to plastic deformation is a tantalizing goal. This is a notion that has long eluded predictions of plastic deformation in crystals, where structural descriptions of defects and obstacles are more apt. The non-equilibrium nature of MGs and its special property of kinetic frustration at low temperatures, leading to glass transition, apparently correlates with destabilization by means of mechanical energy. The broad spectrum of structural states in which a glass can exist, which is a result of its structural heterogeneity and rugged potential energy landscape, is a unique characteristic that allows for a wide range of mechanical behavior. This tunability is appealing from a structural materials perspective, in which a given

glass chemistry can be designed, for instance, for formability or environmental concerns, and the mechanical behavior could be subsequently varied by relatively low energy processing approaches.

In this paper, we have shown that Pt-based MG nanowires subjected to ion irradiation and annealing treatments embody these principles and can be taken to extreme structural states, from well relaxed to heavily rejuvenated, approaching a liquid-like state. Our systematic experimental study using quantitative *in situ* tensile testing shows the influence of irradiation conditions on inelastic response, which is captured well by a unified analytical model that incorporates the structural state of the glass. Specifically, we draw the following conclusions:

- Pt-based MG nanowires produced by thermoplastic molding using nanoscale templates exhibit high strengths, brittle-like tensile behavior and failure mediated by shear banding. Ion irradiation of these nanowires changes the structural state by further disordering the glass, leading to significant tensile ductility, quasi-homogeneous plastic deformation and measurable reductions in yield strength. Sub-T_g annealing of ion-irradiated nanowires elicits structural relaxation and returns the glass state to its as-molded condition and corresponding mechanical behavior. Our systematic study over a range of ion fluences (0–300 ions nm^{-2}) and irradiated volume fraction (0–0.1) suggests that ion fluence and consequent damage show stronger correlations with yield strength reductions over the ranges studied.
- Structural characterization by selected-area transmission electron microscopy diffraction shows subtle changes in the integrated intensity profiles, suggesting a more disordered or liquid-like state in ion-irradiated nanowires. Despite very small differences in scattering signatures, the yield strength reductions are as large as 0.5 GPa.
- Whereas previously reported universal scaling laws linking the yield strength of a given MG and T_g cannot adequately describe the changes in yield strength as a result of ion irradiation and annealing, our newly developed analytical model incorporating the structural state enables predictive capability and captures our results well. We estimate that ion irradiation at high fluence levels (~300 ions/nm^2) lead to changes in T_f of over 100 K, which corresponds to approximately ten orders of magnitude in cooling rate in bulk MGs. We demonstrate the robustness of our model by applying it to literature reports of hardness reductions from severe plastic deformation of MGs, and show that the changes in mechanical properties can be used to adequately predict the excess enthalpies of the glass subjected to varying plastic strain.

Our results not only show that the mechanical properties and plastic deformation mode of small-scale MGs can be varied substantially within a given glass system, but also demonstrate the diversity of processing routes that can be used to tailor the structural properties of MGs. Our results and analysis could potentially be used to design new processing treatments that lead to a broader library of properties and more graceful failure modes in glassy materials.

Acknowledgements

We gratefully acknowledge financial support from the National Science Foundation through PENN MRSEC DMR-1120901, and start-up funding from the University of Pennsylvania. The work of J.S. and G.K. was primarily supported by the National Science Foundation under MRSEC DMR-1119826. D.J.M. acknowledges support from the National Science Foundation Graduate Research Fellowship Program under Grant No: DGE-1321851. We thank the Penn Nanoscale Characterization Facility for technical support. We also thank P. Derlet, A. Liu and R.W. Carpick for insightful discussions.

References

[1] Klement W, Willens RH, Duwez P. Non-crystalline structure in solidified gold–silicon alloys. Nature 1960;187(4740):869–70. http://dx.doi.org/10.1038/187869b0. <http://www.nature.com/nature/journal/v187/n4740/abs/187869b0>.

[2] Ashby M, Greer A. Metallic glasses as structural materials. Scr Mater 2006;54(3):321–6. http://dx.doi.org/10.1016/j.scriptamat.2005.09.051. <http://linkinghub.elsevier.com/retrieve/pii/S1359646205006111>.

[3] Demetriou MD, Launey ME, Garrett G, Schramm JP, Hofmann DC, Johnson WL, et al. A damage-tolerant glass. Nat Mater 2011;10(2):123–8. http://dx.doi.org/10.1038/nmat2930. <http://www.ncbi.nlm.nih.gov/pubmed/21217693>.

[4] Kumar G, Tang HX, Schroers J. Nanomoulding with amorphous metals. Nature 2009;457(7231):868–72. http://dx.doi.org/10.1038/nature07718. <http://www.ncbi.nlm.nih.gov/pubmed/19212407>.

[5] Inoue A, Wang XM, Zhang W. Developmens and applications of bulk metallic glasses. Rev Adv Mater Sci 2008;18:1–9.

[6] Chu JP, Huang JC, Jang JSC, Wang YC, Liaw PK. Thin film metallic glasses: Preparations, properties, and applications. JOM 2010;62(4):19–24. http://dx.doi.org/10.1007/s11837-010-0053-3. <http://www.springerlink.com/index/10.1007/s11837-010-0053-3>.

[7] Greer A, Cheng Y, Ma E. Shear bands in metallic glasses. Mater Sci Eng R Reports 2013;74(4):71–132. http://dx.doi.org/10.1016/j.mser.2013.04.001. <http://linkinghub.elsevier.com/retrieve/pii/S0927796X13000259>.

[8] Argon A. Plastic deformation in metallic glasses. Acta Metall 1979;27(1):47–58. http://dx.doi.org/10.1016/0001-6160(79)90055-5. <http://linkinghub.elsevier.com/retrieve/pii/0001616079900555>.

[9] Schuh C, Hufnagel T, Ramamurty U. Mechanical behavior of amorphous alloys. Acta Mater 2007;55(12):4067–109. http://dx.doi.org/10.1016/j.actamat.2007.01.052. <http://linkinghub.elsevier.com/retrieve/pii/S135964540700122X>.

[10] Lu J, Ravichandran G, Johnson W. Deformation behavior of the Zr41.2Ti13.8Cu12.5Ni10Be22.5 bulk metallic glass over a wide range of strain-rates and temperatures. Acta Mater 2003;51(12):3429–43. http://dx.doi.org/10.1016/S1359-6454(03)00164-2. <http://linkinghub.elsevier.com/retrieve/pii/S1359645403001642>.

[11] Spaepen F. A microscopic mechanism for steady state inhomogeneous flow in metallic glasses. Acta Metall 1977;25(4):407–15. http://dx.doi.org/10.1016/0001-6160(77)90232-2. <http://linkinghub.elsevier.com/retrieve/pii/0001616077902322>.

[12] Langer J. Dynamics of shear-transformation zones in amorphous plasticity: formulation in terms of an effective disorder temperature. Phys Rev E 2004;70(4):041502. http://dx.doi.org/10.1103/Phys

RevE.70.041502. <http://link.aps.org/doi/10.1103/PhysRevE.70.041502>.
[13] van den Beukel A, Sietsma J. The glass transition as a free volume related kinetic phenomenon. Acta Metall Mater 1990;38(3):383–9. http://dx.doi.org/10.1016/0956-7151(90)90142-4. <http://www.sciencedirect.com/science/article/pii/095671519090>.
[14] Slipenyuk A, Eckert J. Correlation between enthalpy change and free volume reduction during structural relaxation of Zr55Cu30Al10Ni5 metallic glass. Scr Mater 2004;50(1):39–44. http://dx.doi.org/10.1016/j.scriptamat.2003.09.038. <http://linkinghub.elsevier.com/retrieve/pii/S1359646203005979>.
[15] Zhao YY, Zhao X. Structural relaxation and its influence on the elastic properties and notch toughness of Mg–Zn–Ca bulk metallic glass. J Alloys Compd 2012;515:154–60. http://dx.doi.org/10.1016/j.jallcom.2011.11.125. <http://dx.doi.org/10.1016/j.jallcom.2011.11.125>.
[16] Berthier L, Barrat JL. Shearing a glassy material: numerical tests of nonequilibrium mode-coupling approaches and experimental proposals. Phys Rev Lett 2002;89(9):095702. http://dx.doi.org/10.1103/PhysRevLett.89.095702. <http://link.aps.org/doi/10.1103/PhysRevLett.89.095702>.
[17] Shi Y, Katz M, Li H, Falk M. Evaluation of the disorder temperature and free-volume formalisms via simulations of shear banding in amorphous solids. Phys Rev Lett 2007;98(18):185505. http://dx.doi.org/10.1103/PhysRevLett.98.185505. <http://link.aps.org/doi/10.1103/PhysRevLett.98.185505>.
[18] Turnbull D. Under what conditions can a glass be formed? Contemp Phys 1969;10(5):473–88. <http://www.tandfonline.com/doi/abs/10.1080/00107516908204405>.
[19] Egami T, Waseda Y. Atomic size effect on the formability of metallic glasses. J Non Cryst Solids 1984;64(1–2):113–34. http://dx.doi.org/10.1016/0022-3093(84)90210-2. <http://www.sciencedirect.com/science/article/pii/002230938490>.
[20] Inoue A. Stabilization of metallic supercooled liquid and bulk amorphous alloys. Acta Mater 2000;48(1):279–306. http://dx.doi.org/10.1016/S1359-6454(99)00300-6. <http://linkinghub.elsevier.com/retrieve/pii/S1359645499003006>.
[21] Lu Z, Liu C. A new glass-forming ability criterion for bulk metallic glasses. Acta Mater 2002;50(13):3501–12. http://dx.doi.org/10.1016/S1359-6454(02)00166-0. <http://linkinghub.elsevier.com/retrieve/pii/S1359645402001660>.
[22] Lewandowski JJ, Wang WH, Greer AL. Intrinsic plasticity or brittleness of metallic glasses. Philos Mag Lett 2005;85(2):77–87. http://dx.doi.org/10.1080/09500830500080474. <http://www.tandfonline.com/doi/abs/10.1080/09500830500080474>.
[23] Schroers J, Johnson W. Ductile bulk metallic glass. Phys Rev Lett 2004;93(25):255506. http://dx.doi.org/10.1103/PhysRevLett.93.255506. <http://link.aps.org/doi/10.1103/PhysRevLett. 93.255506>.
[24] Gilbert CJ, Ritchie RO, Johnson WL. Fracture toughness and fatigue-crack propagation in a Zr–Ti–Ni–Cu–Be bulk metallic glass. Appl Phys Lett 1997;71(4):476. http://dx.doi.org/10.1063/1.119610. <http://link.aip.org/link/APPLAB/v71/i4/p476/s1&Agg=doi>.
[25] Kumar G, Rector D, Conner R, Schroers J. Embrittlement of Zr-based bulk metallic glasses. Acta Mater 2009;57:3572–83. http://dx.doi.org/10.1016/j.actamat.2009.04.016. <http://linkinghub.elsevier.com/retrieve/pii/S1359645409002365>.
[26] Kumar G, Prades-Rodel S, Blatter A, Schroers J. Unusual brittle behavior of Pd-based bulk metallic glass. Scr Mater 2011;65(7):585–7. http://dx.doi.org/10.1016/j.scriptamat.2011.06.029. <http://linkinghub.elsevier.com/retrieve/pii/S1359646211003575>.
[27] Lund AC, Schuh CA. Yield surface of a simulated metallic glass. Acta Mater 2003;51(18):5399–411. http://dx.doi.org/10.1016/S1359-6454(03)00396-3. <http://linkinghub.elsevier.com/retrieve/pii/S1359645403003963>.
[28] Song K, Pauly S, Zhang Y, Scudino S, Gargarella P, Surreddi K, et al. Significant tensile ductility induced by cold rolling in Cu47.5Zr47.5Al5 bulk metallic glass. Intermetallics 2011;19(10):1394–8. http://dx.doi.org/10.1016/j.intermet.2011.05.001. <http://linkinghub.elsevier.com/retrieve/pii/S0966979511001348>.
[29] Lu J, Ravichandran G. Pressure-dependent flow behavior of Zr41.2Ti13.8Cu12.5Ni10Be22.5 bulk metallic glass. J Mater Res 2003;18(09):2039–49. http://dx.doi.org/10.1557/JMR.2003.0287. <http://www.journals.cambridge.org/abstract_S0884291400064396>.
[30] Murali P, Ramamurty U. Embrittlement of a bulk metallic glass due to sub-annealing. Acta Mater 2005;53(5):1467–78. http://dx.doi.org/10.1016/j.actamat.2004.11.040. <http://linkinghub.elsevier.com/retrieve/pii/S1359645404007256>.
[31] Kumar G, Neibecker P, Liu YH, Schroers J. Critical fictive temperature for plasticity in metallic glasses. Nat Commun 2013;4:1536. http://dx.doi.org/10.1038/ncomms2546. <http://www.nature.com/doifinder/10.1038/ncomms2546>.
[32] Tool AQ. Relation between inelastic deformability and thermal expansion of glass in its annealing range. J Am Ceram Soc 1946;29(9):240–53. http://dx.doi.org/10.1111/j.1151-2916.1946.tb11592.x. <http://doi.wiley.com/10.1111/j.1151-2916.1946.tb11592.x>.
[33] Packard CE, Witmer LM, Schuh CA. Hardening of a metallic glass during cyclic loading in the elastic range. Appl Phys Lett 2008;92(17):171911. http://dx.doi.org/10.1063/1.2919722. <http://link.aip.org/link/APPLAB/v92/i17/p171911/s1&Agg=doi>.
[34] Packard C, Homer E, Al-Aqeeli N, Schuh CA. Cyclic hardening of metallic glasses under Hertzian contacts: experiments and STZ dynamics simulations. Philos Mag 2010;90(10):1373–90. http://dx.doi.org/10.1080/14786430903352664. <http://www.tandfonline.com/doi/abs/10.1080/14786430903352664>.
[35] Lo Y, Chou H, Cheng Y, Huang J, Morris J, Liaw P. Structural relaxation and self-repair behavior in nano-scaled Zr–Cu metallic glass under cyclic loading: molecular dynamics simulations. Intermetallics 2010;18(5):954–60. http://dx.doi.org/10.1016/j.intermet.2010.01.012. <http://linkinghub.elsevier.com/retrieve/pii/ S0966979510000233>.
[36] Tong P, Louca D, Wang G, Liaw PK, Maxey E, Yokoyama Y. The effects of fatigue on the atomic structure with cyclic loading in Zr50Cu40Al10 and Zr60Cu30Al10 glasses. Metall Mater Trans A 2011;43(8):2676–9. http://dx.doi.org/10.1007/s11661-011-0887-5. <http://link.springer.com/10.1007/s11661-011-0887-5>.
[37] Deng C, Schuh CA. Atomistic mechanisms of cyclic hardening in metallic glass. Appl Phys Lett 2012;100(25):251909. http://dx.doi.org/10.1063/1.4729941. <http://link.aip.org/link/APPLAB/v100/i25/p251909/s1&Agg=doi>.
[38] Takayama S. Drawing of Pd77.5Cu6Si16.5 metallic glass wires. Mater Sci Eng 1979;38(1):41–8. http://dx.doi.org/10.1016/0025-5416(79)90030-2. <http://linkinghub.elsevier.com/retrieve/pii/0025541679900302>.
[39] Dmowski W, Yokoyama Y, Chuang A, Ren Y, Umemoto M, Tsuchiya K, et al. Structural rejuvenation in a bulk metallic glass induced by severe plastic deformation. Acta Mater 2010;58(2):429–38. http://dx.doi.org/10.1016/j.actamat.2009.09.021. <http://linkinghub.elsevier.com/retrieve/pii/S135964540900617X>.
[40] Scudino S, Jerliu B, Surreddi K, Kühn U, Eckert J. Effect of cold rolling on compressive and tensile mechanical properties of Zr52.5Ti5Cu18Ni14.5Al10 bulk metallic glass. J Alloys Compd 2011;509:S128–30. http://dx.doi.org/10.1016/j.jallcom.2011.01.022. <http://linkinghub.elsevier.com/retrieve/pii/S0925838811000624>.
[41] Wang X, Cao Q, Jiang J, Franz H, Schroers J, Valiev R, et al. Atomic-level structural modifications induced by severe plastic shear deformation in bulk metallic glasses. Scr Mater 2011;64(1):81–4. http://dx.doi.org/10.1016/j.scriptamat.2010.09.015. <http://linkinghub.elsevier.com/retrieve/pii/S1359646210006330>.
[42] Meng F, Tsuchiya K, Yokoyama Y. Reversible transition of deformation mode by structural rejuvenation and relaxation in bulk metallic glass. Appl Phys Lett 2012;101(12):121914. http://dx.doi.org/10.1063/1.4753998. <http://link.aip.org/link/APPLAB/v101/i12/p121914/s1&Agg=doi>.
[43] Zhilyaev a, Langdon T. Using high-pressure torsion for metal processing: fundamentals and applications. Prog Mater Sci

2008;53(6):893–979. http://dx.doi.org/10.1016/j.pmatsci.2008.03.002. <http://linkinghub.elsevier.com/retrieve/pii/S007964250800025X>.
[44] Zhang Y, Wang WH, Greer AL. Making metallic glasses plastic by control of residual stress. Nat Mater 2006;5(11):857–60. http://dx.doi.org/10.1038/nmat1758. <http://www.ncbi.nlm.nih.gov/pubmed/17041581>.
[45] Raghavan R, Ayer R, Jin H, Marzinsky C, Ramamurty U. Effect of shot peening on the fatigue life of a Zr-based bulk metallic glass. Scr Mater 2008;59(2):167–70. http://dx.doi.org/10.1016/j.scriptamat.2008.03.009. <http://linkinghub.elsevier.com/retrieve/pii/ S1359646208002133>.
[46] Concustell A, Méar F, Suriñach S, Baró M, Greer A. Structural relaxation and rejuvenation in a metallic glass induced by shot-peening. Philos Mag Lett 2009;89(12):831–40. http://dx.doi.org/10.1080/09500830903337919. <http://www.tandfonline.com/doi/abs/10.1080/09500830903337919>.
[47] Gerling R, Schimansky F, Wagner R. Restoration of the ductility of thermally embrittled amorphous alloys under neutron-irradiation. Acta Metall 1987;35(5):1001–6. http://dx.doi.org/10.1016/0001-6160(87)90047-2. <http://linkinghub.elsevier.com/retrieve/pii/0001616087900472>.
[48] Mayr S. Impact of ion irradiation on the thermal, structural, and mechanical properties of metallic glasses. Phys Rev B 2005;71(14):1–7. http://dx.doi.org/10.1103/PhysRevB.71.144109. <http://link.aps.org/doi/10.1103/PhysRevB.71.144109>.
[49] Xiao Q, Huang L, Shi Y. Suppression of shear banding in amorphous ZrCuAl nanopillars by irradiation. J Appl Phys 2013;113(8):083514. http://dx.doi.org/10.1063/1.4793562. <http://link.aip.org/link/JAPIAU/v113/i8/p083514/s1&Agg=doi>.
[50] Avchaciov KA, Ritter Y, Djurabekova F, Nordlund K, Albe K. Controlled softening of Cu64Zr36 metallic glass by ion irradiation. Appl Phys Lett 2013;102(18):181910. http://dx.doi.org/10.1063/1.4804630. <http://link.aip.org/link/APPLAB/v102/i18/p181910/s1&Agg=doi>.
[51] Raghavan R, Boopathy K, Ghisleni R, Pouchon M, Ramamurty U, Michler J. Ion irradiation enhances the mechanical performance of metallic glasses. Scr Mater 2010;62(7):462–5. http://dx.doi.org/10.1016/j.scriptamat.2009.12.013. <http://linkinghub.elsevier.com/retrieve/pii/S1359646209007660>.
[52] Raghavan R, Kombaiah B, Döbeli M, Erni R, Ramamurty U, Michler J. Nanoindentation response of an ion irradiated Zr-based bulk metallic glass. Mater Sci Eng A 2012;532:407–13. http://dx.doi.org/10.1016/j.msea.2011.11.004. <http://linkinghub.elsevier.com/retrieve/pii/S0921509311012159>.
[53] Liu YH, Zhao F, Li YL, Chen MW. Deformation behavior of metallic glass thin films. J Appl Phys 2012;112(6):063504. http://dx.doi.org/10.1063/1.4752280. <http://link.aip.org/link/JAPIAU/v112/i6/p063504/s1&Agg=doi>.
[54] Magagnosc DJ, Ehrbar R, Kumar G, He MR, Schroers J, Gianola DS. Tunable tensile ductility in metallic glasses. Sci Rep 2013;3:16–8. http://dx.doi.org/10.1038/srep01096. <http://www.nature.com/doifinder/10.1038/srep01096>.
[55] Chen DZ, Jang D, Guan KM, An Q, Goddard Wa, Greer JR. Nanometallic glasses: size reduction brings ductility, surface state drives its extent. Nano Lett 2013;13(9):4462–8. http://dx.doi.org/10.1021/nl402384r. <http://www.ncbi.nlm.nih.gov/pubmed/23978318>.
[56] Schuster B, Wei Q, Ervin M, Hruszkewycz S, Miller M, Hufnagel T, et al. Bulk and microscale compressive properties of a Pd-based metallic glass. Scr Mater 2007;57(6):517–20. http://dx.doi.org/10.1016/j.scriptamat.2007.05.025. <http://linkinghub.elsevier.com/retrieve/pii/S1359646207003806>.
[57] Guo H, Yan PF, Wang YB, Tan J, Zhang ZF, Sui ML, et al. Tensile ductility and necking of metallic glass. Nat Mater 2007;6(10):735–9. http://dx.doi.org/10.1038/nmat1984. <http://www.ncbi.nlm.nih.gov/pubmed/17704779>.
[58] Lee CJ, Huang JC, Nieh TG. Sample size effect and microcompression of Mg[sub 65]Cu[sub 25]Gd[sub 10] metallic glass. Appl Phys Lett 2007;91(16):161913. http://dx.doi.org/10.1063/1.2800313. <http://link.aip.org/link/APPLAB/v91/i16/p161913/s1&Agg=doi>.
[59] Lai Y, Lee C, Cheng Y, Chou H, Chen H, Du X, et al. Bulk and microscale compressive behavior of a Zr-based metallic glass. Scr Mater 2008;58(10):890–3. http://dx.doi.org/10.1016/j.scriptamat.2008.01.009. <http://linkinghub.elsevier.com/retrieve/pii/S1359646208000389>.
[60] Volkert CA, Donohue A, Spaepen F. Effect of sample size on deformation in amorphous metals. J Appl Phys 2008;103(8):083539. http://dx.doi.org/10.1063/1.2884584. <http://link.aip.org/link/JAPIAU/v103/i8/p083539/s1&Agg=doi>.
[61] Dubach A, Raghavan R, Loffler J, Michler J, Ramamurty U. Micropillar compression studies on a bulk metallic glass in different structural states. Scr Mater 2009;60:567–70. http://dx.doi.org/10.1016/j.scriptamat.2008.12.013. <http://linkinghub.elsevier.com/retrieve/pii/S1359646208008592>.
[62] Jang D, Greer J. Transition from a strong-yet-brittle to a stronger-and-ductile state by size reduction of metallic glasses. Nat Mater 2010;9(3):1–5. http://dx.doi.org/10.1038/nmatnmat2622. <http://dx.doi.org/10.1038/nmatnmat2622>.
[63] Chen C, Pei Y, De Hosson J. Effects of size on the mechanical response of metallic glasses investigated through in situ TEM bending and compression experiments. Acta Mater 2010;58(1):189–200. http://dx.doi.org/10.1016/j.actamat.2009.08.070. <http://linkinghub.elsevier.com/retrieve/pii/S1359645409005928>.
[64] Chen C, Pei Y, Kuzmin O, Zhang Z, Ma E, De Hosson J. Intrinsic size effects in the mechanical response of taper-free nanopillars of metallic glass. Phys Rev B 2011;83(18):4–7. http://dx.doi.org/10.1103/PhysRevB.83.180201. <http://link.aps.org/doi/10.1103/PhysRevB.83.180201>.
[65] Tian L, Cheng YQ, Shan ZW, Li J, Wang CC, Han XD, et al. Approaching the ideal elastic limit of metallic glasses. Nat Commun 2012;3:609. http://dx.doi.org/10.1038/ncomms1619. <http://www.pubmedcentral.nih.gov/articlerender.fcgi?artid=327>.
[66] Gianola DS, Sedlmayr A, Mönig R, Volkert CA, Major RC, Cyrankowski E, et al. In situ nanomechanical testing in focused ion beam and scanning electron microscopes. Rev Sci Instrum 2011;82(6):063901. http://dx.doi.org/10.1063/1.3595423. <http://www.ncbi.nlm.nih.gov/pubmed/21721703>.
[67] Murphy KF, Chen LY, Gianola DS. Effect of organometallic clamp properties on the apparent diversity of tensile response of nanowires. Nanotechnology 2013;24(23):235704. http://dx.doi.org/10.1088/0957-4484/24/23/235704. <http://www.ncbi.nlm.nih.gov/pubmed/23669193>.
[68] Agrawal R, Bernal RA, Isheim D, Espinosa HD. Characterizing atomic composition and dopant distribution in wide band gap semiconductor nanowires using laser-assisted atom probe tomography. J Phys Chem C 2011;115(36):17688–94. http://dx.doi.org/10.1021/jp2047823. <http://pubs.acs.org/doi/abs/10.1021/jp2047823>.
[69] Sigmund P. A mechanism of surface micro-roughening by ion bombardment. J Mater Sci 1973;8(11):1545–53. http://dx.doi.org/10.1007/BF00754888. <http://link.springer.com/10.1007/BF00754888>.
[70] Schultz P, Lynn K. Interaction of positron beams with surfaces, thin films, and interfaces. Rev Mod Phys 1988;60(3):701–79. http://dx.doi.org/10.1103/RevModPhys.60.701. <http://link.aps.org/doi/10.1103/RevModPhys.60.701>.
[71] Donth EJ. The glass transition: relaxation dynamics in liquids and disordered materials. Berlin: Springer; 2001. ISBN 3540418016 9783540418016.
[72] Badrinarayanan P, Zheng W, Li Q, Simon SL. The glass transition temperature versus the fictive temperature. J Non Cryst Solids 2007;353(26):2603–12. http://dx.doi.org/10.1016/j.jnoncrysol.2007.04.025. <http://linkinghub.elsevier.com/retrieve/pii/S0022309307004103>.
[73] Debenedetti PG, Stillinger FH. Supercooled liquids and the glass transition. Nature 2001;410(6825):259–67. http://dx.doi.org/10.1038/35065704. <http://www.ncbi.nlm.nih.gov/pubmed/11258381>.
[74] Brüning R, Samwer K. Glass transition on long time scales. Phys Rev B 1992;46(18):318–22. <http://prb.aps.org/abstract/PRB/v46/i18/p11318_1>.
[75] Freed R, Vander Sande J. The metallic glass Cu56Zr44: devitrification and the effects of devitrification on mechanical properties. Acta Metall 1980;28(1):103–21. http://dx.doi.org/10.1016/0001-6160(80)90044-9. <http://linkinghub.elsevier.com/retrieve/pii/0001616080900449>.

[76] Luo Q, Zhang B, Zhao DQ, Wang RJ, Pan MX, Wang WH. Aging and stability of cerium-based bulk metallic glass. Appl Phys Lett 2006;(15):151915. http://dx.doi.org/10.1063/1.2196231. <http://link.aip.org/link/APPLAB/v88/i15/p151915/s1&Agg=doi>.

[77] Qiao J, Pelletier J. Enthalpy relaxation in Cu46Zr45Al7Y2 and Zr55Cu30Ni5Al10 bulk metallic glasses by differential scanning calorimetry (DSC). Intermetallics 2011;19(1):9–18. http://dx.doi.org/10.1016/j.intermet.2010.08.042. <http://linkinghub.elsevier.com/retrieve/pii/S0966979510003833>.

[78] Moynihan CT, Easteal AJ, Bolt MA, Tucker J. Dependence of the fictive temperature of glass on cooling rate. J Am Ceram Soc 1976;59(1–2):12–6. http://dx.doi.org/10.1111/j.1151-2916.1976.tb09376.x. <http://onlinelibrary.wiley.com/doi/10.1111/j.1151-2916.1976.t>.

[79] Yue Y, Christiansen J, Jensen S. Determination of the fictive temperature for a hyperquenched glass. Chem Phys Lett 2002;357(1–2):20–4. http://dx.doi.org/10.1016/S0009-2614(02)00434-7. <http://linkinghub.elsevier.com/retrieve/pii/S0009261402004347>.

[80] Hammond VH, Houtz MD, O'Reilly JM. Structural relaxation in a bulk metallic glass. J Non Cryst Solids 2003;325(1–3):179–86. http://dx.doi.org/10.1016/S0022-3093(03)00311-9. <http://linkinghub.elsevier.com/retrieve/pii/S0022309303003119>.

[81] Yue Y, von der Ohe R, Jensen SL. Fictive temperature, cooling rate, and viscosity of glasses. J Chem Phys 2004;120(17):8053–9. http://dx.doi.org/10.1063/1.1689951. <http://www.ncbi.nlm.nih.gov/pubmed/15267724>.

[82] Moynihan C. Structural relaxation and the glass transition. Rev Min Geochem 1995;32(1). <http://rimg.geoscienceworld.org/content/32/1/1.short>.

[83] Evenson Z, Gallino I, Busch R. The effect of cooling rates on the apparent fragility of Zr-based bulk metallic glasses. J Appl Phys 2010;107(12):123529. http://dx.doi.org/10.1063/1.3452381. <http://link.aip.org/link/JAPIAU/v107/i12/p123529/s1&Agg=doi>.

[84] Zhu ZG, Wen P, Wang DP, Xue RJ, Zhao DQ, Wang WH. Characterization of flow units in metallic glass through structural relaxations. J Appl Phys 2013;114(8):083512. http://dx.doi.org/10.1063/1.4819484. <http://link.aip.org/link/JAPIAU/v114/i8/p083512/s1&Agg=doi>.

[85] Demkowicz M, Argon A. Liquid like atomic environments act as plasticity carriers in amorphous silicon. Phys Rev B 2005;72(24):245205. http://dx.doi.org/10.1103/PhysRevB.72.245205. <http://link.aps.org/doi/10.1103/PhysRevB.72.245205>.

[86] Ye JC, Lu J, Liu CT, Wang Q, Yang Y. Atomistic free-volume zones and inelastic deformation of metallic glasses. Nat Mater 2010;9(8):619–23. http://dx.doi.org/10.1038/nmat2802. <http://www.ncbi.nlm.nih.gov/pubmed/20651805>.

[87] Yang B, Liu CT, Nieh TG. Unified equation for the strength of bulk metallic glasses. Appl Phys Lett 2006;88(22):221911. http://dx.doi.org/10.1063/1.2206099. <http://link.aip.org/link/APPLAB/v88/i22/p221911/s1&Agg=doi>.

[88] Liu Y, Liu C, Wang W, Inoue A, Sakurai T, Chen M. Thermodynamic origins of shear band formation and the universal scaling law of metallic glass strength. Phys Rev Lett 2009;103(6):065504. http://dx.doi.org/10.1103/PhysRevLett.103.065504. <http://link.aps.org/doi/10.1103/PhysRevLett.103.065504>.

[89] Guan P, Chen M, Egami T. Stress-temperature scaling for steady-state flow in metallic glasses. Phys Rev Lett 2010;104(20):205701. http://dx.doi.org/10.1103/PhysRevLett.104.205701. <http://link.aps.org/doi/10.1103/PhysRevLett.104.205701>.

[90] Gu J, Song M, Ni S, Guo S, He Y. Effects of annealing on the hardness and elastic modulus of a Cu36Zr48Al8Ag8 bulk metallic glass. Mater Des 2013;47:706–10. http://dx.doi.org/10.1016/j.matdes.2012.12.071. <http://linkinghub.elsevier.com/retrieve/pii/S0261306913000022>.

[91] Gallino I, Shah MB, Busch R. Enthalpy relaxation and its relation to the thermodynamics and crystallization of the Zr58.5Cu15.6-Ni12.8Al10.3Nb2.8 bulk metallic glass-forming alloy. Acta Mater 2007;55(4):1367–76. http://dx.doi.org/10.1016/j.actamat.2006.09.040. <http://linkinghub.elsevier.com/retrieve/pii/S1359645406007245>.

[92] Adam G, Gibbs JH. On the temperature dependence of cooperative relaxation properties in glass-forming liquids. J Chem Phys 1965;43(1):139. http://dx.doi.org/10.1063/1.1696442. <http://link.aip.org/link/JCPSA6/v43/i1/p139/s1&Agg=doi>.

[93] Legg BA, Schroers J, Busch R. Thermodynamics, kinetics, and crystallization of Pt57.3Cu14.6Ni5.3P22.8 bulk metallic glass. Acta Mater 2007;55(3):1109–16. http://dx.doi.org/10.1016/j.actamat.2006.09.024. <http://linkinghub.elsevier.com/retrieve/pii/S135964540600704X>.

[94] Nishiyama N, Horino M, Haruyama O, Inoue A. Undercooled liquid-to-glass transition during continuous cooling in Pd–Cu–Ni–P alloys. Appl Phys Lett 2000;76(26):3914. http://dx.doi.org/10.1063/1.126819. <http://link.aip.org/link/APPLAB/v76/i26/p3914/s1&Agg=doi>.

[95] Sargent P, Donovan P. Measurements of the microhardness of metallic glasses compared with some theoretical predictions. Scr Metall 1982;16(11):1207–12. http://dx.doi.org/10.1016/0036-9748(82)90468-9. <http://linkinghub.elsevier.com/retrieve/pii/0036974882904689>.

[96] Schroers J, Johnson WL. Highly processable bulk metallic glass-forming alloys in the Pt–Co–Ni–Cu–P system. Appl Phys Lett 2004;84(18):3666. http://dx.doi.org/10.1063/1.1738945. <http://link.aip.org/link/APPLAB/v84/i18/p3666/s1&Agg=doi>.